Available online at www.sciencedirect.com
ScienceDirect
Precambrian Research 158 (2007) 93–118
Precambrian Research
www.elsevier.com/locate/precamres

Geochemistry and geochronology of high-grade rocks from the Grove Mountains, East Antarctica: Evidence for an Early Neoproterozoic basement metamorphosed during a single Late Neoproterozoic/Cambrian tectonic cycle

Xiaochun Liu [a,*], Bor-Ming Jahn [b,c], Yue Zhao [a], Guochun Zhao [d], Xiaohan Liu [e]

[a] *Institute of Geomechanics, Chinese Academy of Geological Sciences, 11 Minzudaxue Nanlu, Beijing 100081, China*
[b] *Institute of Earth Sciences, Academia Sinica, Taipei 11529, Taiwan*
[c] *Department of Geological Sciences, National Taiwan University, Taipei 106, Taiwan*
[d] *Department of Earth Sciences, The University of Hong Kong, Pokfulam Road, Hong Kong*
[e] *Institute of Geology and Geophysics, Chinese Academy of Sciences, Beijing 100029, China*

Received 30 May 2006; received in revised form 8 April 2007; accepted 24 April 2007

Abstract

The Grove Mountains of East Antarctica are an inland continuation of the Prydz Belt. The high-grade metamorphic complex in this area is composed of felsic orthogneisses and mafic granulites, with minor paragneisses and calc-silicate rocks. U–Pb zircon analyses using SHRIMP and LA-ICP-MS techniques reveal that the protoliths of mafic granulites and felsic orthogneisses were emplaced during a short time interval of ca. 920–910 Ma. Mafic granulites can be divided into low- and high-Ti groups. They have initial ε_{Nd} values [$\varepsilon_{Nd}(T)$] ranging from +0.8 to −1.9. TiO_2 is positively correlated with FeO^t/MgO and La/Nb ratios, whereas it shows a negative correlation with $\varepsilon_{Nd}(T)$ values, indicating that the petrogenesis of their protoliths involved partial melting of a weakly enriched subcontinental lithospheric mantle and fractional crystallization of the magma accompanied by minor crustal contamination. Felsic orthogneisses have an affinity of A_2-type granites, characterized by enrichment in REE, Y, Zr, Th and Ga and high Ga/Al and Y/Nb ratios. Most of them have $\varepsilon_{Nd}(T)$ values of −0.7 to −3.5 and Nd depleted mantle model ages (T_{DM}) of 1.76–1.65 Ga, and a few have low $\varepsilon_{Nd}(T)$ values of −10.4 to −10.6 and old T_{DM} of 2.46–2.27 Ga, reflecting a heterogeneity in their source region. Their protoliths were probably produced by high-temperature partial melting of tonalitic–granodioritic rocks triggered by the underplating of mantle-derived mafic magma during post-orogenic extension. U–Pb analyses also reveal a metamorphic age of ca. 2050 Ma from detrital zircons in a paragneiss, suggesting that the sedimentary materials of the paragneiss may have come from an as yet undiscovered Early Paleoproterozoic orogen of unknown provenance. Voluminous mafic–felsic intrusives and a small amount of sedimentary rocks constitute an Early Neoproterozoic basement of the Grove Mountains. Subsequently, this basement experienced only a single Late Neoproterozoic/Cambrian metamorphic cycle at ca. 550–535 Ma. The available data indicate that the Prydz Belt is a collage of multiple basement terranes and each of them has a distinct tectonic evolution. This supports the suggestion that the Prydz Belt may represent a Late Neoproterozoic/Cambrian collisional orogen that resulted in the final phase of the Gondwana assembly.

Keywords: Early Neoproterozoic; Mafic–felsic intrusion; Late Neoproterozoic/Cambrian; Single metamorphic cycle; Grove Mountains; Prydz Belt; East Antarctica

* Corresponding author. Tel.: +86 10 68486756; fax: +86 10 68422326.
E-mail address: liuxchqw@yahoo.com.cn (X. Liu).

0301-9268/$ – see front matter © 2007 Elsevier B.V. All rights reserved.
doi:10.1016/j.precamres.2007.04.005

1. Introduction

Unravelling the nature of tectonothermal events in a complex orogenic belt is a difficult issue. This is particularly true for the case of the Prydz Belt [also termed Pinjarra Orogen (Fitzsimons, 2003) or Kuunga Orogen (Boger et al., 2002)] in East Antarctica. In this belt, Archaean, Late Mesoproterozoic/Early Neoproterozoic (ca. 1000 Ma) and Late Neoproterozoic/Cambrian (ca. 550 Ma) events have been identified in different localities, but the polyphase deformation, metamorphism and magmatism have provoked a debate on the extent, process and role of each event and therefore on the formation models of the supercontinents Rodinia and Gondwana (Fitzsimons, 2003; Harley, 2003; Yoshida et al., 2003; Zhao et al., 2003). Since the Prydz Belt is situated in the interior of the previously proclaimed unified East Gondwana, some important questions about its evolution emerge: (1) How did the earlier crust in the belt and adjacent areas evolve? (2) What was the nature of the Late Mesoproterozoic/Early Neoproterozoic precursor of the belt and its relationship to other terranes of similar age in the East Antarctic Shield? (3) Were there any geological events recorded in the belt during the time interval of 1000–550 Ma? And most importantly, (4) Whether the Late Neoproterozoic/Cambrian orogeny represented a suture resulted from the collision between two continental blocks, or an intraplate reworking belt in response to the collision in the East African Orogen?

The Grove Mountains are situated about 200 km east of the southern Prince Charles Mountains (SPCM) (Fig. 1). They are considered as an inland continuation of the Prydz Belt based on a few published Cambrian age data (Zhao et al., 2000, 2003; Mikhalsky et al., 2001a). However, the Precambrian crustal history of this area remains poorly constrained. Lithologically, the Grove Mountains mainly comprise high-grade metamorphic rocks and abundant intrusive charnockites and granites. The metamorphic rocks are dominated by orthopyroxene-bearing felsic orthogneisses and mafic granulites, with minor garnet-bearing paragneisses and calc-silicate rocks (Liu et al., 2002; X.H. Liu et al., 2003; X.C. Liu et al., 2003). In this paper we report the result of geochemical and geochronological study on these rocks. We demonstrate that the protoliths of both mafic granulites and felsic orthogneisses are the Early Neoproterozoic post-orogenic intrusives, but not the Late Mesoproterozoic igneous complexes as revealed in the Prydz Bay and eastern Amery Ice Shelf (EAIS) (Y. Wang et al., 2003; Liu et al., 2007). In conjunction with an Early Paleoproterozoic detrital zircon age obtained from a paragneiss, we interpret that the Grove Mountains represent a distinct basement terrane, which was metamorphosed during a single Late Neoproterozoic/Cambrian tectonic cycle. This interpretation may help us to better understand the tectonic evolution of the Prydz Belt in the context of the Gondwana assembly.

2. Geological setting

The Prince Charles Mountains–Prydz Bay area comprises three Archaean cratonic blocks, a Late Mesoproterozoic Fisher Terrane, an Early Neoproterozoic Rayner Complex and a Late Neoproterozoic/Cambrian Prydz Belt (Fig. 1). The three Archaean blocks are exposed in the SPCM, Vestfold Hills and Rauer Group. Each of them preserves distinct crustal histories and therefore is unlikely to represent remnants of a single unified craton (Harley, 2003). The Fisher Terrane crops out in the southern sector of the northern Prince Charles Mountains (NPCM), where mafic–felsic volcanism and intrusion occurred at 1300–1020 Ma, followed by amphibolite facies metamorphism at 1020–940 Ma (Beliatsky et al., 1994; Kinny et al., 1997; Mikhalsky et al., 1999). The Rayner Complex occurs in the NPCM and adjacent Mawson Coast. It is characterized by regional granulite facies metamorphism accompanied by widespread charnockitic and granitic magmatism at ca. 990–980 Ma (Manton et al., 1992; Kinny et al., 1997; Young et al., 1997; Zhao et al., 1997; Boger et al., 2000; Carson et al., 2000). A limited magmatic activity also took place in the area at ca. 940–900 Ma, which was considered as a protraction of the Early Neoproterozoic orogenic event (Boger et al., 2000; Carson et al., 2000). In addition, intraplate deformation and emplacement of minor planar pegmatites at ca. 550–500 Ma were observed in some places (Carson et al., 2000; Boger et al., 2002). This may be a response to the intense Late Neoproterozoic/Cambrian tectonism occurred in the Prydz Belt.

The Prydz Belt crops out along the Prydz Bay coastline, and extends southward through the EAIS to the Grove Mountains (Fitzsimons, 2003; Zhao et al., 2003). The high-grade metamorphic rocks in the Prydz Bay–EAIS area comprise two lithological associations, mafic–felsic composite orthogneisses and migmatitic paragneisses that were termed Søstrene Orthogneiss and Brattstrand Paragneiss and were referred to the basement and cover sequences, respectively (Fitzsimons and Harley, 1991; Carson et al., 1995; Fitzsimons, 1997). Geochronological studies in the Larsemann Hills and the McKaskle Hills suggest that the Søstrene Orthogneiss was emplaced during 1170–1020 Ma (Y. Wang et al., 2003; Liu et al., 2007), while the Brattstrand Paragneiss

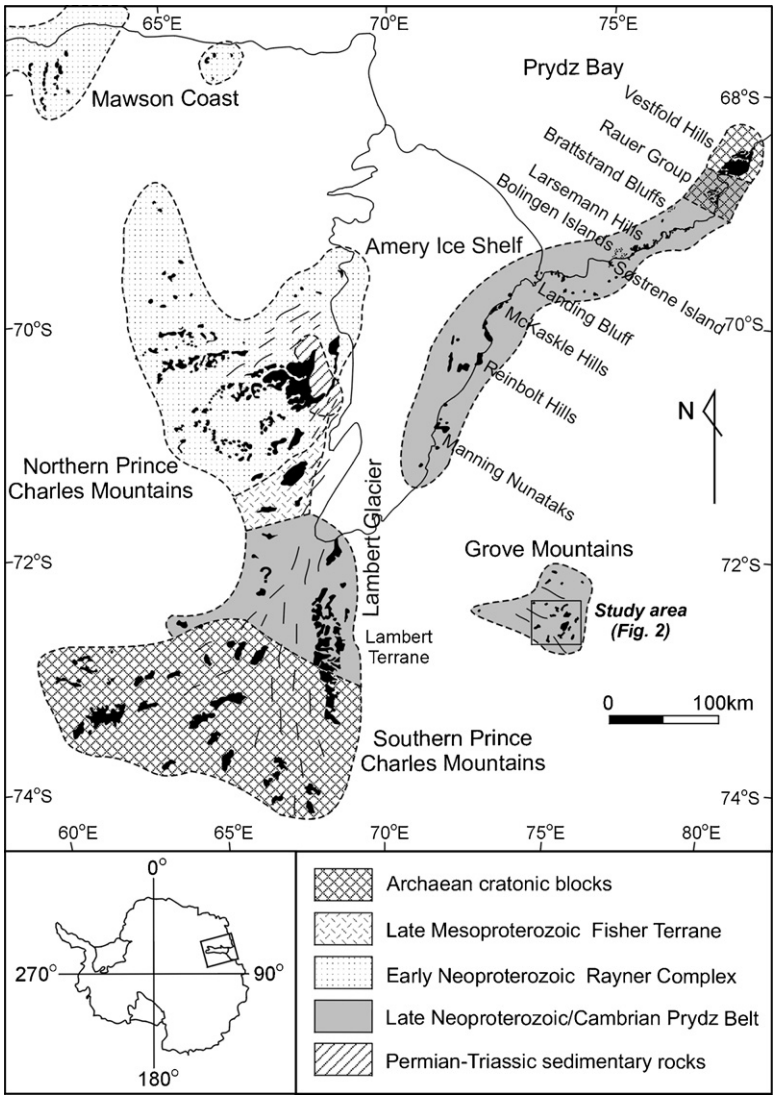

Fig. 1. Geological sketch map of the Prince Charles Mountains–Prydz Bay area and its location in East Antarctica (modified after Mikhalsky et al., 2001b; Fitzsimons, 2003).

is assumed to have deposited during the Late Mesoproterozoic (Dirks and Wilson, 1995; Carson et al., 1996) or Neoproterozoic (Hensen and Zhou, 1995; Zhao et al., 1995). High-grade metamorphism, compressional and subsequent extensional deformation, and emplacement of syn- to post-orogenic granites are constrained to have occurred between 550 and 490 Ma (Zhao et al., 1992, 1995; Hensen and Zhou, 1995; Carson et al., 1996; Fitzsimons et al., 1997). However, high-pressure (10 kbar at 980 °C) metamorphism at ca. 990 Ma was also identified in a garnet-bearing mafic granulite from Søstrene Island (Hensen and Zhou, 1995). Moreover, Late Neoproterozoic/Cambrian ages have also been reported for the Archaean basement rocks in the Rauer Group (Kinny et al., 1993; Harley et al., 1998; Kelsey et al., 2003) and SPCM (Boger et al., 2001).

Similar to the Prydz Bay–EAIS area, the Grove Mountains are also characterized by high-temperature granulite facies metamorphism. The metamorphic rock associations consist mainly of felsic orthogneisses and mafic granulites, with very rare quartzofeldspathic paragneisses and calc-silicate rocks. Until the present study, no systematic geochronological study has been conducted on mafic granulites, ortho- and paragneisses except that an inherited age of 910 Ma for zircon cores and a metamorphic age of 529 ± 14 Ma for zircon rims were obtained using SHRIMP analysis for a felsic orthogneiss (sample MN1-5) collected from Melwold

Nunataks (Zhao et al., 2000). On the other hand, the Grove Mountains contain voluminous intrusive granitoids, including foliated charnockite, sheeted granite and charnockitic and granitic dykes. These granitoids were dated at 547–501 Ma (Zhao et al., 2000; Liu et al., 2006). The origin of the rocks was considered to be related to the underplating of mantle-derived magmas during the extension of the Late Neoproterozoic/Cambrian orogenesis (Liu et al., 2006).

3. Samples

In order to understand the nature and origin of the early igneous event, seven mafic granulites and ten felsic orthogneisses were selected for detailed geochemical study (Fig. 2). Moreover, seven representative samples including three mafic granulites, three felsic orthogneisses and one paragneiss were chosen for U–Pb zircon dating so as to define the timing of igneous, metamorphic and sedimentary events. The sample locations, mineral assemblages and field characteristics are summarized in Table 1.

Mafic granulites are volumetrically minor but are widespread in the Grove Mountains. Most of them occur as small irregular blocks, bands, or interlayers of a few centimeters to 2 m wide in felsic orthogneisses, with reaching 15 m at Melwold Nunataks and 30–50 m at Mason Peaks. Some mafic granulites also occur as large layered enclaves in granitic bodies. Most granulite samples exhibit an equilibrium paragenesis of clinopyroxene + orthopyroxene + hornblende + plagioclase + magnetite − ilmenite, with minor biotite and quartz. However, a significant amount of K-feldspar (mode up to 15%) is found in two samples (ZR1-2 and ZR2-5) from Zakharoff Ridge. Moreover, sample BN7-2 is actually a K-feldspar-bearing amphibolite, which is distinguished from others by the absence of both clino- and orthopyroxenes.

Felsic orthogneisses (i.e., granitic gneisses) are the principal lithological type of the Grove Mountains. They typically show a weak foliation. Almost all primary magmatic minerals and grain fabrics were obliterated by the granulite facies metamorphism and deformation. The present mineral assemblage is composed of biotite + plagioclase + K-feldspar + quartz + magnetite − ilmenite intergrowth, with or without minor orthopyroxene, hornblende and garnet. In sample MN1-5, small garnets occur as inclusions in K-feldspar crystals; they have high MnO contents (7.5–9.5%), seem to form prior to the peak granulite facies metamorphism.

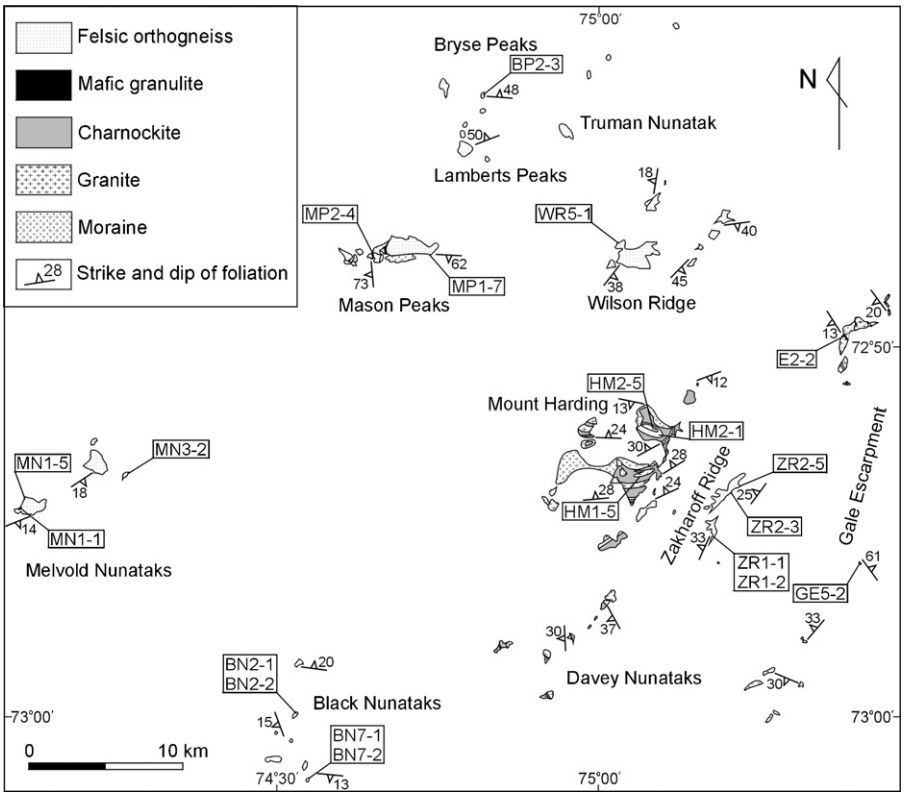

Fig. 2. Geological map of the Grove Mountains showing sampling localities.

Table 1
Locations, mineral assemblages, field characteristics and dating method of the studied samples from the Grove Mountains

Rock type	Sample	Location	Mineral assemblage	Field characteristics	Dating method
Mafic granulite	E2-2	Gale Escarpment	Cpx, Opx, Hbl, Bt, Pl, Qtz, Mag/Ilm	Large enclaves in granite	
	HM2-5	Mount Harding	Cpx, Opx, Hbl, Bt, Pl, Qtz, Mag/Ilm	Large enclaves in granite	
	MP2-4	Mason Peaks	Cpx, Opx, Hbl, Bt, Pl, Qtz, Mag/Ilm	Layer 30 m wide within felsic orthogneiss	SHRIMP
	MN3-2	Melvold Nunataks	Cpx, Opx, Hbl, Bt, Pl, Qtz, Mag/Ilm	Band 70 cm wide within felsic orthogneiss	
	BN7-2	Black Nunataks	Hbl, Bt, Pl, Kfs, Qtz, Mag/Ilm, Ttn	Folded band 20 cm wide within felsic orthogneiss	
	ZR1-2	Zakharoff Ridge	Cpx, Opx, Hbl, Bt, Pl, Kfs, Qtz, Mag/Ilm	Band 10–100 cm wide within felsic orthogneiss	SHRIMP
	ZR2-5	Zakharoff Ridge	Cpx, Opx, Hbl, Bt, Pl, Kfs, Qtz, Mag/Ilm	Band 10–100 cm wide within felsic orthogneiss	
	MN1-1	Melvold Nunataks	Cpx, Opx, Hbl, Bt, Pl, Qtz, Mag/Ilm	Layer 15 m wide within felsic orthogneiss	SHRIMP
Felsic orthogneiss	ZR1-1	Zakharoff Ridge	Opx, Bt, Pl, Kfs, Qtz, Mag/Ilm	Covered an outcrop with granulite bands	SHRIMP
	ZR2-3	Zakharoff Ridge	Grt, Opx, Bt, Pl, Kfs, Qtz, Mag/Ilm	Covered an outcrop	
	GE5-2	Gale Escarpment	Opx, Hbl, Bt, Pl, Kfs, Qtz, Mag/Ilm	Covered an outcrop intruded by charnockitic dyke	
	HM2-1	Mount Harding	Opx, Bt, Pl, Kfs, Qtz, Mag/Ilm	Thick layer intruded by sheeted granite	
	WR5-1	Wilson Ridge	Opx, Hbl, Bt, Pl, Kfs, Qtz, Mag/Ilm	Covered an outcrop	
	MP1-7	Mason Peaks	Opx, Hbl, Bt, Pl, Kfs, Qtz, Mag/Ilm	Covered an outcrop with granulite layers	SHRIMP
	MN1-5	Melvold Nunataks	Grt, Bt, Pl, Kfs, Qtz, Mag/Ilm	Covered an outcrop	SHRIMP (Zhao et al., 2000)
	BN2-1	Black Nunataks	Opx, Bt, Pl, Kfs, Qtz, Mag/Ilm	Covered an outcrop	
	BN2-2	Black Nunataks	Bt, Pl, Kfs, Qtz, Mag/Ilm	Intercalated layer within BN2-1	
	BN7-1	Black Nunataks	Hbl, Bt, Pl, Kfs, Qtz, Mag/Ilm	Covered an outcrop with granulite bands	
	HM1-5	Mount Harding	Bt, Pl, Kfs, Qtz, Mag/Ilm	Lens surrounded by mafic granulite and granite	LA-ICP-MS
Paragneiss	BP2-3	Bryse Peaks	Grt, Bt, Pl, Qtz, Ilm, Spl	Layer 50 m wide intercalated in felsic orthogneiss	LA-ICP-MS

Abbreviations: Bt, biotite; Cpx, clinopyroxene; Grt, garnet; Hbl, hornblende; Ilm, ilmenite; Kfs, K-feldspar; Mag, magnetite; Opx, orthopyroxene; Pl, plagioclase; Qtz, quartz; Spl, spinel; Ttn, titanite.

Sample HM1-5 was collected from a felsic orthogneiss lens enclosed in between mafic granulite and sheeted granite at Mount Harding. It contains numerous larger quartz crystals with inclusions of fine-grained biotite, plagioclase and K-feldspar. The paragenesis suggests a late recrystallization of the quartz.

The dated sample BP2-3 is a typical paragneiss seldom occurring in the Grove Mountains. The rock occurs as an interlayer of 50 m wide in felsic orthogneiss and has mineral assemblage of garnet + biotite + plagioclase + quartz, with minor spinel and ilmenite.

4. Analytical techniques

4.1. Whole-rock geochemical analyses

Major and trace element abundances were measured by XRF (3080E) and ICP-MS (TJA PQ ExCell), respectively, at the National Research Center for Geo-

analysis, Chinese Academy of Geological Sciences. FeO was separately determined by wet chemical method. Detailed analytical procedures for ICP-MS analysis were described by L. Wang et al. (2003). Analytical uncertainties range from ±1 to ±5% for major elements, ±5% for trace elements with concentrations ≥20 ppm and ±10% for concentrations ≤20 ppm. The chondritic values used in construction of REE patterns and the primitive mantle (PM) values used in spidergrams are from Sun and McDonough (1989).

4.2. Sr–Nd isotopic analyses

Sr–Nd isotopic analyses were performed at the Institute of Geology and Geophysics, Chinese Academy of Sciences. The analytical procedures are the same as reported by Liu et al. (2006). Sm–Nd model ages (T_{DM}) were calculated assuming a linear isotopic evolution of the depleted mantle reservoir from $\varepsilon_{Nd}(T) = 0$ at 4.56 Ga to +10 at the present. The equation is:

$$T_{DM} = \frac{1}{\lambda_{Sm}} \ln \left\{ 1 + \frac{(^{143}Nd/^{144}Nd)_s - 0.51315}{(^{147}Sm/^{144}Nd)_s - 0.2137} \right\},$$

where s is the sample and λ_{Sm} is the decay constant of ^{147}Sm ($0.00654\,Ga^{-1}$).

4.3. Zircon U–Pb analyses

Sensitive high-resolution ion microprobe (SHRIMP) and laser ablation inductively coupled plasma mass spectrometer (LA-ICP-MS) were employed for zircon U–Pb analyses. Zircons were extracted using the conventional techniques, including crushing, sieving, heavy liquid and hand picking. Internal structures of zircon grains were revealed by cathodoluminescence (CL) imaging. SHRIMP analyses were performed at the Beijing SHRIMP Centre, Chinese Academy of Geological Sciences. Instrumental conditions and data acquisition procedures are the same as described by Williams (1998). The measured $^{206}Pb/^{238}U$ ratios were corrected using reference zircon TEMORA (416.75 ± 0.24 Ma; Black et al., 2003). Correction for common Pb was made using the measured ^{204}Pb. LA-ICP-MS analyses were conducted at the Key Laboratory of Continental Dynamics, Northwest University, China. Instrumental conditions and analytical details were reported by Yuan et al. (2004). The measured $^{206}Pb/^{238}U$ ratios were corrected using reference zircon 91500 (1065.4 ± 0.6 Ma; Wiedenbeck et al., 1995). Correction for common Pb was applied using the method of Anderson (2002). Ages were calculated using the ISOPLOT program (version 2.06; Ludwig, 1999). The age uncertainties for individual analyses represent one standard deviation (1σ), but the calculated weighted mean $^{206}Pb/^{238}U$ or $^{207}Pb/^{206}Pb$ ages are quoted at 2σ.

5. Geochemistry

5.1. Major and trace elements

Major and trace element compositions of mafic granulites and felsic orthogneisses are listed in Table 2 . The mafic granulites cover a narrow range of SiO_2 contents, from 47 to 49%. They can be divided into two groups based on their Ti contents. Granulites of the low-Ti group have TiO_2 contents of 1.7–2.8% and K_2O contents of

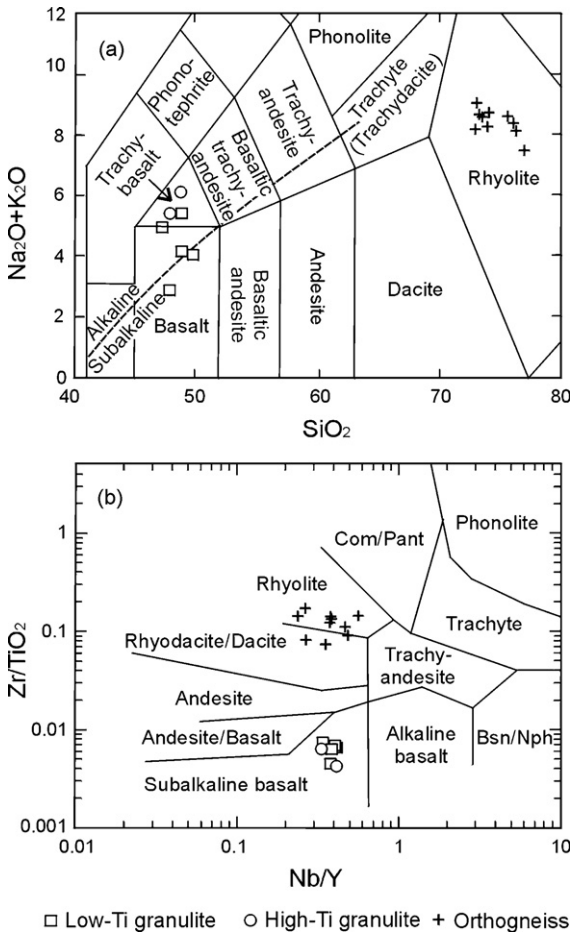

Fig. 3. (a) Total alkali vs. SiO_2 diagram for classification of mafic granulites and felsic orthogneisses from the Grove Mountains (after Middlemost, 1994). (b) Zr/TiO_2 vs. Nb/Y diagram for classification of mafic granulites and felsic orthogneisses from the Grove Mountains (after Winchester and Floyd, 1977). Note that all mafic granulites fall in the subalkaline basalt field in (b), but most fall in the alkaline basalt field in (a), suggesting the mobile signature of alkaline elements during the high-grade metamorphism.

Table 2
Chemical compositions of mafic granulites and felsic orthogneisses from the Grove Mountains

	Rock type																
	Low-Ti granulite					High-Ti granulite		Felsic orthogneiss									
	E2-2	HM2-5	MP2-4	MN3-2	BN7-2	ZR1-2	ZR2-5	ZR1-1	ZR2-3	GE5-2	HM2-1	WR5-1	MP1-7	MN1-5	BN2-1	BN2-2	BN7-1
SiO_2 (wt%)	47.49	46.78	48.64	49.37	48.20	48.22	46.97	72.58	72.98	72.35	72.17	75.29	73.46	73.19	75.67	75.24	76.62
TiO_2	1.68	2.29	2.43	2.77	1.71	4.44	4.64	0.32	0.27	0.33	0.36	0.25	0.29	0.25	0.21	0.14	0.15
Al_2O_3	14.64	14.90	14.91	13.38	14.35	10.88	11.91	13.36	13.72	12.72	13.95	12.12	12.78	13.62	12.19	13.02	12.20
Fe_2O_3	3.86	2.85	2.76	2.58	2.42	2.64	3.00	1.64	1.20	1.32	1.41	1.06	1.55	0.56	1.07	1.16	0.42
FeO	8.55	11.08	10.69	11.93	9.86	14.26	13.04	1.10	0.93	1.72	0.74	0.81	1.02	1.42	0.57	0.16	0.74
MnO	0.21	0.22	0.25	0.24	0.23	0.26	0.25	0.04	0.03	0.04	0.04	0.03	0.04	0.18	0.03	0.03	0.02
MgO	8.15	6.98	5.48	5.16	6.66	4.53	3.98	0.14	0.18	0.37	0.26	0.13	0.17	0.26	0.15	0.08	0.30
CaO	11.68	8.67	10.00	9.51	9.69	6.62	7.98	1.07	1.37	1.19	1.81	0.98	1.20	1.17	1.09	0.99	1.55
Na_2O	2.39	3.36	3.19	3.30	3.63	2.38	2.49	3.04	3.50	2.80	3.50	2.84	2.99	3.14	2.91	3.12	3.12
K_2O	0.45	1.57	0.97	0.76	1.75	3.68	2.82	5.94	5.04	5.76	4.59	5.47	5.68	5.06	5.14	5.44	4.36
P_2O_5	0.15	0.21	0.22	0.26	0.18	1.11	1.12	0.05	0.08	0.07	0.08	0.03	0.05	0.04	0.05	0.04	0.02
LOI	1.19	1.09	0.76	0.63	0.91	0.66	1.13	0.29	0.54	0.66	0.47	0.41	0.39	0.43	0.31	0.53	0.31
Total	100.44	100.00	100.30	99.89	99.59	99.68	99.33	99.57	99.84	99.33	99.38	99.42	99.62	99.32	99.39	99.95	99.81
K_2O/Na_2O	0.19	0.47	0.30	0.23	0.48	1.55	1.13	1.95	1.44	2.06	1.31	1.93	1.90	1.61	1.77	1.74	1.40
A/CNK	0.57	0.65	0.61	0.57	0.56	0.55	0.55	1.00	1.00	0.98	0.99	0.98	0.96	1.07	0.99	1.02	0.96
A/NK	3.31	2.06	2.37	2.14	1.82	1.38	1.67	1.17	1.22	1.17	1.30	1.14	1.15	1.28	1.18	1.18	1.24
Mg#	57	50	45	42	52	35	33	10	15	20	20	13	12	21	16	12	35
Rb (ppm)	4.43	105	12.1	8.37	91.3	207	121	222	173	155	211	224	180	212	185	216	185
Sr	337	286	302	240	153	213	356	66.8	77.9	78.7	119	71.8	82.5	104	98.8	65.8	140
Ba	118	346	237	120	89.4	981	832	650	589	1128	825	413	967	987	609	362	579
Pb	3.53	15.4	12.1	17.2	15.7	10.1	14.0	34.9	38.3	33.8	37.4	31.2	41.2	42.9	36.8	42.8	37.5
Th	0.18	2.64	2.13	1.63	5.18	0.45	0.52	39.7	33.8	27.8	12.3	19.8	33.6	39.7	18.0	13.6	19.2
U	<0.05	0.63	0.51	0.50	2.72	0.05	0.20	2.89	3.79	1.60	2.02	2.57	2.76	3.41	2.50	5.18	2.17
Zr	73.3	156	156	182	126	193	296	371	217	421	320	281	340	417	150	146	188
Hf	2.41	4.12	4.33	5.09	3.59	5.18	6.92	12.1	6.74	11.5	9.36	8.45	9.72	12.4	4.66	4.39	7.64
Nb	8.51	12.6	13.4	17.0	14.9	22.9	17.3	17.7	9.19	19.0	15.8	15.0	19.9	23.5	4.55	7.14	14.5
Ta	0.64	0.66	1.04	1.21	1.01	1.21	0.70	0.91	0.55	0.86	0.59	0.76	1.05	1.74	0.17	0.18	1.07
Sc	39.9	29.0	42.4	40.7	39.8	38.9	36.2	3.88	3.78	7.05	3.33	3.70	4.39	9.02	3.25	3.11	2.79
V	329	362	463	425	321	318	355	7.47	10.2	6.62	12.6	3.24	7.47	9.15	7.45	6.10	5.56
Cr	197	151	105	59.1	159	31.1	39.9	3.24	4.08	9.36	5.37	1.9	1.85	3.26	3.26	3.26	1.28
Co	51.6	63.8	43.2	45.5	54.9	52.1	43.0	2.04	2.19	2.54	2.47	1.54	1.98	1.98	2.01	1.13	2.32
Ni	63.2	130	32.8	31.1	55.5	23.5	19.9	1.17	1.42	6.08	3.18	1.41	0.93	1.98	1.64	1.23	4.32
Cu	25.3	33.0	53.6	34.5	4.80	11.4	33.1	4.35	2.22	4.14	6.32	2.18	3.25	14.5	5.65	2.41	6.70
Zn	92.3	220	142	167	259	213	233	66.6	36.1	47.6	51.4	33.9	46.7	36.4	30.0	27.0	30.1
Ga	20.6	23.4	25.3	23.6	33.5	27.2	23.5	27.8	24.3	20.4	27.3	20.4	22.0	22.7	20.4	21.1	25.4
Y	22.6	31.0	34.4	41.1	43.2	55.6	51.5	45.4	35.2	33.2	32.3	40.3	52.0	93.0	13.1	15.2	64.4

Table 2 (*Continued*)

	Rock type																
	Low-Ti granulite					High-Ti granulite		Felsic orthogneiss									
	E2-2	HM2-5	MP2-4	MN3-2	BN7-2	ZR1-2	ZR2-5	ZR1-1	ZR2-3	GE5-2	HM2-1	WR5-1	MP1-7	MN1-5	BN2-1	BN2-2	BN7-1
Th/U		4.2	4.2	3.3	1.9	8.9	2.6	13.7	8.9	17.4	6.1	7.7	12.2	11.6	7.2	2.6	8.8
10000 Ga/Al	2.66	2.97	3.21	3.33	4.41	4.72	3.73	3.93	3.35	3.03	3.70	3.18	3.25	3.15	3.16	3.06	3.93
Y/Nb	2.66	2.46	2.57	2.42	2.90	2.43	2.98	2.56	3.83	1.75	2.04	2.69	2.61	3.96	2.88	2.13	4.44
La	11.6	19.2	19.6	24.2	22.0	38.4	37.8	81.0	66.8	61.6	71.0	84.2	101	81.1	46.5	30.7	45.1
Ce	26.5	40.1	43.1	55.1	56.2	86.3	83.9	166	134	155	156	145	209	145	87.8	58.0	99.2
Pr	3.93	5.63	6.20	7.68	6.83	12.8	10.7	21.1	17.5	11.5	16.3	18.5	22.1	18.8	10.4	7.10	12.2
Nd	16.8	24.8	25.1	32.0	27.0	53.9	48.6	80.3	65.7	42.1	59.7	66.2	70.5	67.9	37.1	26.1	46.2
Sm	3.74	5.76	5.35	6.73	5.69	11.0	10.9	14.8	11.9	7.50	9.54	10.6	13.2	10.8	6.47	5.08	10.1
Eu	1.38	1.88	1.77	2.10	1.36	2.81	3.21	1.24	0.76	1.84	1.23	0.98	1.59	1.40	0.86	0.59	1.02
Gd	4.16	6.12	5.99	7.31	6.31	11.5	11.5	13.5	10.6	7.59	8.16	9.61	12.2	10.1	5.66	5.54	10.2
Tb	0.64	1.00	0.92	1.12	1.03	1.67	1.79	2.14	1.54	1.17	1.12	1.47	1.83	1.71	0.75	0.64	1.91
Dy	4.19	5.82	6.18	7.30	7.02	10.4	10.0	11.6	7.74	6.63	6.04	7.85	10.7	13.0	3.41	3.37	12.2
Ho	0.91	1.21	1.31	1.59	1.60	2.19	2.05	2.19	1.46	1.39	1.23	1.65	2.42	3.80	0.53	0.61	2.72
Er	2.03	3.34	2.93	3.58	3.77	4.78	5.71	4.57	3.21	3.40	2.85	3.77	5.18	11.0	1.30	1.62	6.53
Tm	0.31	0.48	0.45	0.54	0.63	0.71	0.79	0.66	0.46	0.55	0.40	0.59	0.84	2.40	0.15	0.24	1.10
Yb	2.13	2.90	3.17	3.80	4.57	4.90	4.92	3.90	2.71	3.52	2.17	3.48	5.17	18.2	0.88	1.43	6.69
Lu	0.32	0.43	0.45	0.55	0.70	0.72	0.75	0.53	0.39	0.56	0.32	0.51	0.83	3.11	0.13	0.21	0.99
REE	78.63	118.67	122.53	153.59	144.71	242.08	232.62	403.53	324.78	304.36	336.06	354.41	456.55	388.32	201.94	141.23	256.16
$(La/Yb)_N$	3.9	4.7	4.4	4.6	3.5	5.6	5.5	14.9	17.7	12.6	23.5	17.4	14.0	3.2	37.9	15.4	4.8
Eu/Eu^*	1.06	0.96	0.95	0.91	0.69	0.76	0.87	0.26	0.20	0.74	0.42	0.29	0.38	0.40	0.42	0.34	0.30

0.5–1.8%. Their Mg# range from 42 to 57. Granulites of the high-Ti group occur only in Zakharoff Ridge (sample ZR1-2 and ZR2-5) and have TiO_2 = 4.4–4.6% and K_2O = 2.8–3.7%. Their Mg# are relatively low (33–35). Two kinds of mafic granulite are classified as basalts (gabbros) to trachybasalts (monzogabbros) in the total alkali versus silica (TAS) classification by Middlemost (1994) (Fig. 3a). However, they all fall in the subalkaline basalt field on the Nb/Y versus Zr/TiO_2 discrimination of Winchester and Floyd (1977) (Fig. 3b). This suggests that the alkaline elements may have been remobilized during the granulite facies metamorphism. Despite slight differences in rare earth element (REE) abundances, the two groups exhibit similar chondrite-normalized REE distribution patterns (Fig. 4a), characterized by moderate LREE enrichment [$(La/Yb)_N$ = 4–6] and small negative Eu anomalies (Eu/Eu^* = 0.69–0.96 except for sample E2-2 with a small positive Eu anomaly). However, the two groups have different trace element patterns in the primitive mantle normalized spidergrams (Fig. 4b). High-Ti granulites have large negative Nb–Ta and Sr anomalies and positive P and Ti anomalies, whereas low-

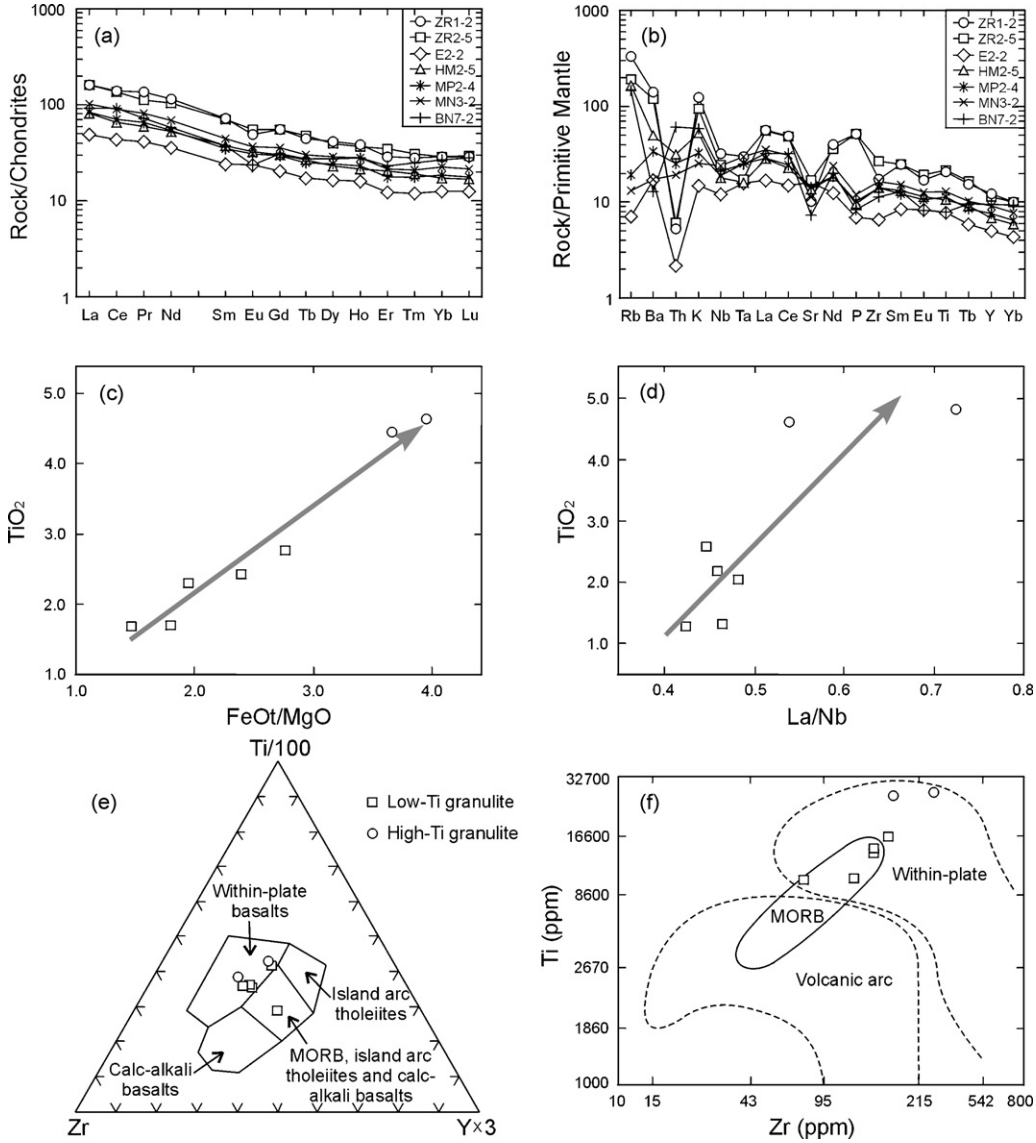

Fig. 4. Diagrams illustrating the chemical characteristics of mafic granulites from the Grove Mountains. (a) Chondrite-normalized REE patterns [chondrite values used for normalization are from Sun and McDonough (1989)]. (b) Primitive mantle (PM) normalized spidergrams [the PM values used for normalization are from Sun and McDonough (1989)]. (c) Plot of TiO_2 vs. FeO^t/MgO. (d) Plot of TiO_2 vs. La/Nb. (e) Ti–Zr–Y discrimination diagram (after Pearce and Cann, 1973). (f) Ti–Zr discrimination diagram (after Pearce and Cann, 1973).

Ti granulites only show moderate depletions of Nb–Ta, Sr (except for sample E2-2) and P. Even so, a positive correlation between TiO_2 contents and FeO^t/MgO and La/Nb ratios could be observed from the total samples (Fig. 4c and d). In addition, Fig. 4b also shows a severe, irregular variation in Rb, Ba and Th abundances, suggesting their mobile nature during the high-grade metamorphism. The Zr, Ti and Y geochemical behavior of both groups of mafic granulite indicates their affinities as within-plate basalts (WPB) (Fig. 4e and f) (Pearce and Cann, 1973).

The felsic orthogneisses belong to the rhyolite (granite) group in the TAS and Nb/Y versus Zr/TiO_2 classification diagrams (see Fig. 3a and b). Their SiO_2 contents range from 72 to 77%, Al_2O_3 from 12 to 14%, and Na_2O/K_2O ratios vary from 1.31 to 2.06. The rocks are metaluminous to peraluminous, with a small range of A/CNK ratios [molar $Al_2O_3/(CaO + Na_2O + K_2O)$] from 0.96 to 1.07, and A/NK ratios [molar $Al_2O_3/(Na_2O + K_2O)$] from 1.14 to 1.30. The chondrite-normalized REE patterns of felsic orthogneisses are moderately or strongly fractionated, with $(La/Yb)_N$ ratios between 3 and 38 (Fig. 5a). They have total REE contents of 141–457 ppm and all show marked negative Eu anomalies ($Eu/Eu^* = 0.20$–0.42; except for sample GE5-2 with a higher Eu/Eu^* value of 0.74). Moreover, sample MN1-5 shows a strong enrichment of HREE, co-respondent to the presence of garnet or other HREE-rich minerals such as xenotime. In the primitive mantle normalized spidergrams (Fig. 5b), all the felsic orthogneisses exhibit high abundances of Rb, Th, K, Zr and La (REE), and relative depletion in Ba,

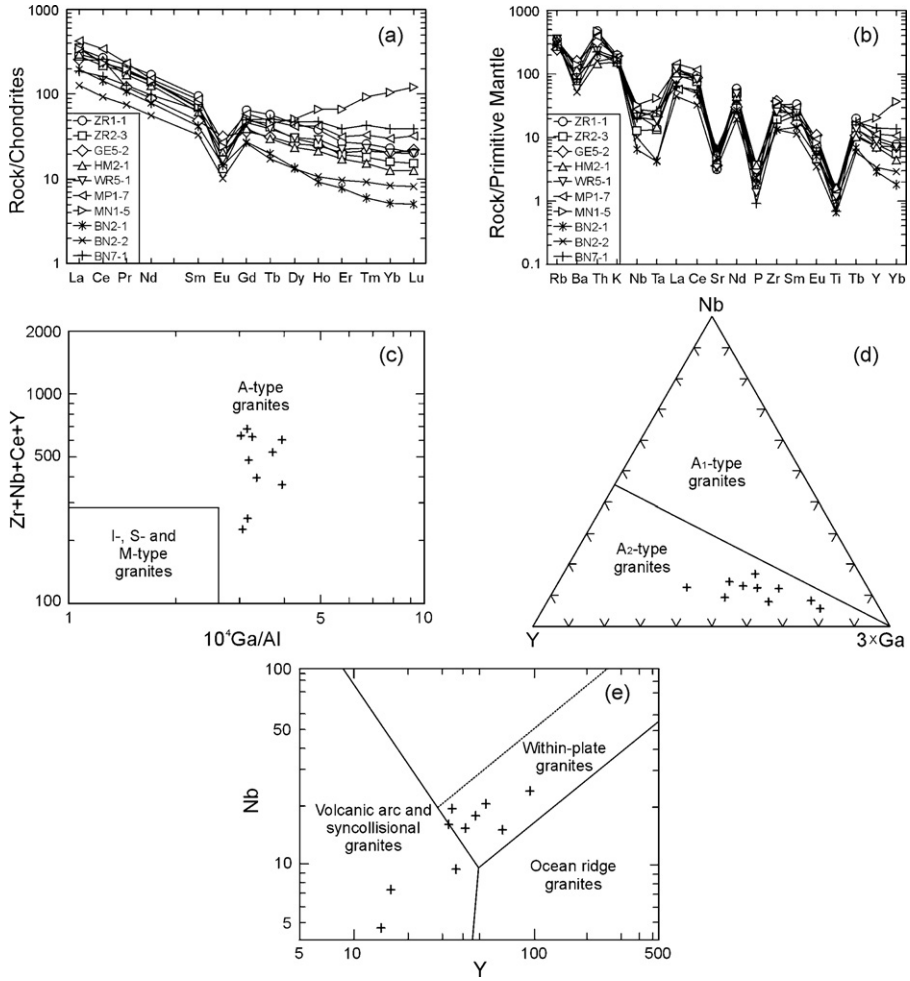

Fig. 5. Diagrams illustrating the chemical characteristics of felsic orthogneisses from the Grove Mountains. (a) Chondrite-normalized REE patterns [chondrite values used for normalization are from Sun and McDonough (1989)]. (b) Primitive mantle (PM) normalized spidergrams [the PM values used for normalization are from Sun and McDonough (1989)]. (c) Plot of 10^4 Ga/Al vs. Zr + Nb + Ce + Y (after Whalen et al., 1987). (d) Y–Nb–3Ga diagram (after Eby, 1992). (d) Plots of Nb vs. Y (after Pearce et al., 1984).

Nb–Ta, Sr, P and Ti. In addition, most samples have Th contents (12–40 ppm) and Th/U ratios (6.1–17.4 except for sample BN2-2) higher than the estimated crustal average (3.8) (Taylor and McLennan, 1985), which are similar to the Mesoproterozoic and Cambrian granitoids from the Prydz Belt (Sheraton and Black, 1988; Sheraton et al., 1996; Liu et al., 2006). Trace element geochemistry also indicates that all the felsic orthogneisses have an affinity of A-type granites, characterized by strong enrichment in Ga, Zr, Nb and Y. 10^4 Ga/Al ratios of the rocks range from 3.03 to 3.93, with an average value of 3.37 (Fig. 5c). Y/Nb ratios range from 1.75 to 4.44, in accord with the A_2-type granites (Fig. 5d; Eby, 1992). In Nb versus Y diagram of Pearce et al. (1984), most samples fall in the field of within-plate granites (WPG), but three samples (BN2-1, BN2-2 and ZR2-3) are found in the field of syncollisional granites (Fig. 5e).

5.2. Sr–Nd isotopes

Rb–Sr and Sm–Nd isotopic data of mafic granulites, felsic orthogneisses and a paragneiss are presented in Table 3. The age-corrected initial $^{87}Sr/^{86}Sr$ ratios (I_{Sr}) range from 0.6995 to 0.7116 for mafic granulites and from 0.7024 to 0.7497 for felsic orthogneisses. Clearly, the Rb–Sr isotopic systems have been disturbed during the high-grade metamorphism, and the calculated I_{Sr} ratios cannot be used to infer the nature of the source region. The initial ε_{Nd} values [$\varepsilon_{Nd}(T)$] range from +0.8 to −0.7 for low-Ti granulites and from −1.8 to −1.9 for high-Ti granulites. Broadly, the TiO_2 contents show a negative correlation with $\varepsilon_{Nd}(T)$ values (Fig. 6a). Felsic orthogneisses mainly have $\varepsilon_{Nd}(T)$ values ranging from −0.7 to −3.5 (Fig. 6b), with Nd depleted mantle model ages (T_{DM}) of 1.76–1.65 Ga (except for sample BN7-1 with T_{DM} = 2.2 Ga), but two samples (GE5-2 and MP1-7) have much lower $\varepsilon_{Nd}(T)$ values (−10.4 to −10.6) and older T_{DM} (2.46–2.27 Ga). The only paragneiss sample (BP2-3) gives a low $\varepsilon_{Nd}(T)$ values of −24.5 (t = 550 Ma) and an Archaean T_{DM} of 2.99 Ga.

6. Geochronology

6.1. SHRIMP results

Three mafic granulites with high-Ti (sample ZR1-2), low-Ti (samples MP2-4) and unknown Ti contents (sample MN1-1) and two felsic orthogneiss with old (sample MP1-7) and young T_{DM} (sample ZR1-1) were chosen for SHRIMP U–Pb zircon analyses. The analytical data are given in Table 4.

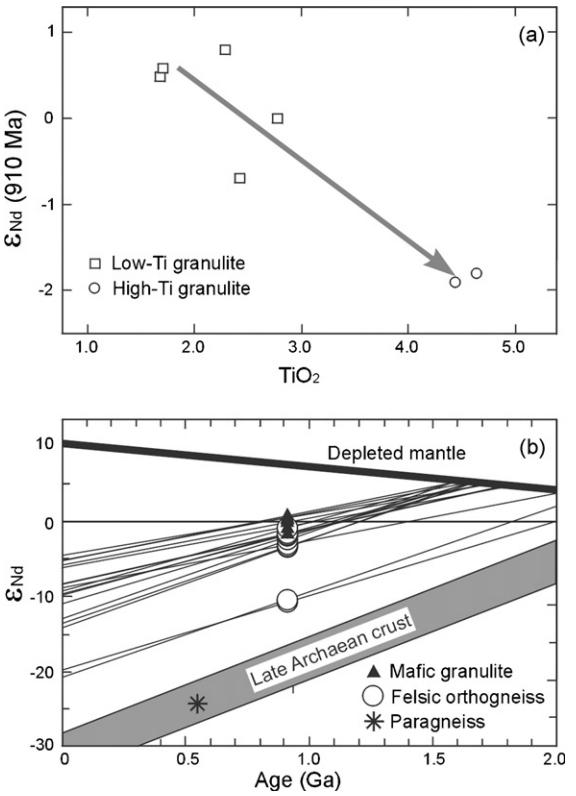

Fig. 6. (a) Plot of initial ε_{Nd}(910 Ma) vs. TiO_2 for mafic granulites from the Grove Mountains. (b) Nd evolution diagram for mafic granulites, felsic orthogneisses and paragneiss from the Grove Mountains.

6.1.1. Sample ZR1-2: mafic granulite

Zircons from sample ZR1-2 are colorless or pale yellow and ovoid to prismatic, with 30–200 μm in length. The CL images reveal that almost all zircon grains have typical core–rim structures (Fig. 7a and b). Some cores are well preserved and exhibit broad oscillatory zoned patterns as typically observed in zircon domains from some gabbros (Rubatto and Gebauer, 2000). Hence, these cores are interpreted to be magmatic in origin. However, the oscillatory bands of most other cores have been thickened and even entirely blurred, suggesting a solid-state recrystallization (Hoskin and Black, 2000). The rims are brightly luminescent and, in some cases, show planar growth banding that are interpreted to have formed during metamorphism (Rubatto and Gebauer, 2000). Thirty-three spot analyses on 30 zircon grains were performed on this sample. All the core analyses were restricted in the well-preserved oscillatory zoned domains. These analyses yielded a very large range of $^{207}Pb/^{206}Pb$ ages from 1907 ± 26 to 562 ± 180 Ma, and their Th/U ratios vary from 0.25 to 0.65. Spots 17.1 and 8.1 gave $^{207}Pb/^{206}Pb$ ages of 1907 ± 26 and 1046 ± 82 Ma, respectively. Both ages are considered

Table 3
Sr–Nd isotopic analyses for mafic granulites, felsic orthogneisses and paragneiss from the Grove Mountains

Sample	Rb (ppm)	Sr (ppm)	$^{87}Rb/^{86}Sr$	$^{87}Sr/^{86}Sr$	I_{Sr}	Sm (ppm)	Nd (ppm)	$^{147}Sm/^{144}Nd$	$^{143}Nd/^{144}Nd$	$\varepsilon_{Nd}(0)$	$\varepsilon_{Nd}(t)$	T_{DM} (Ga)
Low-Ti granulite (t = 910 Ma)												
E2-2	1.5	337.8	0.013	0.705760 ± 15	0.7056	4.01	15.85	0.1533	0.512405 ± 10	−4.5	0.5	1.87
HM2-5	104.6	208.3	1.443	0.718824 ± 16	0.7001	5.81	24.29	0.1447	0.512372 ± 17	−5.2	0.8	1.71
MP2-4	10.7	259.0	0.118	0.710649 ± 15	0.7091	5.63	22.86	0.1492	0.512318 ± 10	−6.2	−0.7	1.96
MN3-2	7.2	205.3	0.101	0.708728 ± 15	0.7074	8.09	33.51	0.1461	0.512336 ± 08	−5.9	0.0	1.83
BN7-2	87.3	138.2	1.817	0.735263 ± 14	0.7116	6.29	25.93	0.1469	0.512371 ± 11	−5.2	0.6	1.77
High-Ti granulite (t = 910 Ma)												
ZR1-2	186.8	185.3	2.904	0.737247 ± 14	0.6995	11.26	48.62	0.1402	0.512202 ± 08	−8.5	−1.9	1.96
ZR2-5	121.8	244.1	1.431	0.722662 ± 15	0.7041	10.89	47.14	0.1398	0.512209 ± 13	−8.4	−1.8	1.93
Felsic orthogneiss (t = 910 Ma)												
ZR1-1	237.8	69.5	9.960	0.850526 ± 15	0.7210	17.19	82.11	0.1267	0.512141 ± 19	−9.7	−1.6	1.76
ZR2-3	218.8	95.7	6.634	0.804918 ± 15	0.7186	14.81	73.44	0.1221	0.512156 ± 13	−9.4	−0.7	1.65
GE5-2	185.5	79.4	6.781	0.827304 ± 13	0.7391	8.22	41.24	0.1207	0.511644 ± 11	−19.4	−10.6	2.46
HM2-1	220.2	151.5	4.196	0.766065 ± 12	0.7115	11.33	64.14	0.1069	0.511922 ± 16	−14.0	−3.5	1.75
WR5-1	232.0	76.8	8.770	0.825159 ± 14	0.7111	13.28	73.54	0.1093	0.511945 ± 17	−13.5	−3.4	1.75
MP1-7	191.8	89.1	6.237	0.800587 ± 17	0.7195	13.73	76.29	0.1089	0.511581 ± 10	−20.6	−10.4	2.27
MN1-5	206.1	105.0	5.665	0.776111 ± 13	0.7024	11.60	65.91	0.1065	0.511983 ± 05	−12.8	−2.3	1.66
BN2-1	178.3	106.6	4.837	0.805807 ± 14	0.7429	7.33	37.56	0.1181	0.512078 ± 18	−10.9	−1.8	1.70
BN2-2	216.4	69.8	9.048	0.867346 ± 15	0.7497	5.26	25.65	0.1242	0.512133 ± 13	−9.9	−1.4	1.73
BN7-1	193.0	157.4	3.528	0.762100 ± 15	0.7162	11.11	45.57	0.1476	0.512183 ± 11	−8.9	−3.2	2.22
Paragneiss (t = 550 Ma)												
BP2-3	137.2	74.8	5.292	0.760981 ± 14	0.7195	9.23	51.77	0.1079	0.511063 ± 10	−30.7	−24.5	2.99

Table 4
SHRIMP U–Pb analyses of zircons for mafic granulites and felsic orthogneisses from the Grove Mountains

Spot	U (ppm)	Th (ppm)	Th/U	Pb^* (ppm)	Common ^{206}Pb (%)	Isotopic ratios			Ages (Ma)	
						$^{206}Pb/^{238}U$	$^{207}Pb/^{235}U$	$^{207}Pb/^{206}Pb$	$^{206}Pb/^{238}U$	$^{207}Pb/^{206}Pb$
Sample ZR1-2 (mafic granulite)										
Oscillatory zoned core										
1.1	69	29	0.44	8.23	1.18	0.1362 ± 0.0035	1.264 ± 0.073	0.0673 ± 0.0035	823 ± 20	846 ± 110
1.2	74	41	0.58	9.51	1.80	0.1476 ± 0.0037	1.437 ± 0.104	0.0707 ± 0.0047	887 ± 21	948 ± 140
2.1	75	36	0.50	9.78	0.57	0.1513 ± 0.0080	1.412 ± 0.095	0.0677 ± 0.0028	908 ± 44	859 ± 86
3.1	142	71	0.52	14.9	0.51	0.1215 ± 0.0028	1.077 ± 0.048	0.0643 ± 0.0024	739 ± 16	750 ± 81
4.1	318	160	0.52	41.5	0.07	0.1516 ± 0.0033	1.394 ± 0.040	0.0667 ± 0.0013	910 ± 18	827 ± 41
5.1	527	242	0.47	65.5	0.10	0.1445 ± 0.0030	1.386 ± 0.037	0.0696 ± 0.0011	870 ± 17	916 ± 32
6.1	240	110	0.47	31.0	0.05	0.1499 ± 0.0034	1.458 ± 0.038	0.0706 ± 0.0009	900 ± 19	945 ± 27
7.1	257	141	0.57	32.9	0.20	0.1483 ± 0.0033	1.405 ± 0.038	0.0687 ± 0.0010	892 ± 18	889 ± 32
8.1	322	161	0.52	43.0	0.11	0.1554 ± 0.0034	1.588 ± 0.073	0.0742 ± 0.0040	931 ± 19	1046 ± 82
9.1	635	152	0.25	59.0	0.12	0.1080 ± 0.0048	0.946 ± 0.043	0.0635 ± 0.0006	661 ± 28	725 ± 22
10.1	195	105	0.56	25.2	0.47	0.1498 ± 0.0033	1.395 ± 0.050	0.0675 ± 0.0020	900 ± 19	855 ± 60
11.1	147	60	0.42	14.5	0.34	0.1146 ± 0.0026	1.018 ± 0.035	0.0644 ± 0.0016	699 ± 15	755 ± 53
12.1	613	248	0.42	71.3	0.15	0.1350 ± 0.0028	1.239 ± 0.030	0.0666 ± 0.0007	816 ± 16	824 ± 22
13.1	222	95	0.44	24.2	0.02	0.1269 ± 0.0028	1.213 ± 0.032	0.0693 ± 0.0010	770 ± 16	908 ± 30
14.1	388	226	0.60	51.7	0.12	0.1549 ± 0.0034	1.469 ± 0.035	0.0688 ± 0.0008	928 ± 19	893 ± 23
15.1	314	154	0.50	37.3	0.08	0.1380 ± 0.0030	1.308 ± 0.033	0.0688 ± 0.0009	833 ± 17	891 ± 27
16.1	248	83	0.35	25.2	0.14	0.1182 ± 0.0026	1.070 ± 0.029	0.0657 ± 0.0010	720 ± 15	797 ± 31
17.1	343	130	0.39	85.1	0.01	0.2884 ± 0.0061	4.642 ± 0.121	0.1168 ± 0.0018	1634 ± 31	1907 ± 26
18.1	182	114	0.65	23.2	0.14	0.1477 ± 0.0163	1.414 ± 0.155	0.0694 ± 0.0011	888 ± 93	912 ± 33
18.2	194	121	0.64	25.5	0.24	0.1521 ± 0.0033	1.402 ± 0.038	0.0669 ± 0.0010	913 ± 19	834 ± 31
19.1	450	244	0.56	61.8	0.29	0.1594 ± 0.0035	1.566 ± 0.052	0.0712 ± 0.0017	954 ± 19	964 ± 49
20.1	217	115	0.55	24.0	0.19	0.1282 ± 0.0028	1.153 ± 0.033	0.0652 ± 0.0012	778 ± 16	781 ± 37
21.1	136	67	0.51	13.0	1.00	0.1104 ± 0.0025	0.896 ± 0.076	0.0589 ± 0.0048	675 ± 15	562 ± 180
22.1	184	83	0.46	23.7	0.07	0.1497 ± 0.0034	1.333 ± 0.039	0.0646 ± 0.0012	899 ± 19	760 ± 38
Brightly luminescent rim										
13.2	188	57	0.31	14.6	0.42	0.0899 ± 0.0021	0.730 ± 0.034	0.0589 ± 0.0024	555 ± 12	564 ± 88
23.1	345	107	0.32	26.7	0.68	0.0893 ± 0.0025	0.734 ± 0.034	0.0595 ± 0.0022	552 ± 15	587 ± 81
24.1	130	36	0.29	9.70	0.20	0.0867 ± 0.0020	0.699 ± 0.026	0.0585 ± 0.0017	536 ± 12	549 ± 63
25.1	134	37	0.29	9.92	0.00	0.0860 ± 0.0037	0.732 ± 0.036	0.0617 ± 0.0015	532 ± 22	665 ± 51
26.1	152	46	0.31	12.2	0.42	0.0927 ± 0.0021	0.698 ± 0.028	0.0546 ± 0.0018	571 ± 13	397 ± 74
27.1	134	41	0.32	9.62	0.40	0.0833 ± 0.0020	0.660 ± 0.031	0.0575 ± 0.0021	516 ± 15	510 ± 79
28.1	127	42	0.34	9.70	0.31	0.0886 ± 0.0021	0.712 ± 0.026	0.0584 ± 0.0016	547 ± 12	543 ± 58
29.1	167	50	0.31	12.4	0.45	0.0865 ± 0.0020	0.679 ± 0.030	0.0569 ± 0.0021	535 ± 12	488 ± 82
30.1	184	68	0.38	14.0	0.57	0.0882 ± 0.0020	0.681 ± 0.033	0.0560 ± 0.0024	545 ± 12	453 ± 96
Sample MP2-4 (mafic granulite)										
Broadly banded or blurred core										
1.1	573	432	0.78	45.1	0.56	0.0911 ± 0.0023	0.813 ± 0.033	0.0647 ± 0.0021	562 ± 14	766 ± 67
2.1	481	1103	2.37	43.8	0.67	0.1053 ± 0.0026	0.857 ± 0.039	0.0590 ± 0.0022	645 ± 16	568 ± 80
3.1	275	775	2.92	27.0	0.95	0.1131 ± 0.0029	0.971 ± 0.052	0.0623 ± 0.0029	691 ± 17	683 ± 100
4.1	426	620	1.51	31.7	0.56	0.0863 ± 0.0022	0.787 ± 0.032	0.0662 ± 0.0021	533 ± 13	812 ± 66
5.1	177	140	0.81	13.2	1.37	0.0854 ± 0.0024	0.730 ± 0.064	0.0620 ± 0.0051	528 ± 14	674 ± 180
6.1	501	697	1.44	52.7	0.31	0.1221 ± 0.0032	1.105 ± 0.041	0.0656 ± 0.0018	742 ± 18	795 ± 57
7.1	332	310	0.96	34.5	0.49	0.1201 ± 0.0031	1.087 ± 0.054	0.0656 ± 0.0028	731 ± 18	794 ± 89
8.1	504	296	0.61	39.1	0.65	0.0897 ± 0.0022	0.821 ± 0.034	0.0664 ± 0.0022	554 ± 13	818 ± 70
9.1	128	237	1.91	10.0	2.78	0.0883 ± 0.0027	0.844 ± 0.118	0.0693 ± 0.0097	546 ± 16	907 ± 280
10.1	467	427	0.95	42.5	0.56	0.1053 ± 0.0023	0.888 ± 0.026	0.0611 ± 0.0012	646 ± 13	644 ± 41
11.1	680	899	1.37	55.2	0.99	0.0936 ± 0.0023	0.758 ± 0.033	0.0587 ± 0.0021	577 ± 14	556 ± 76
12.1	129	181	1.45	9.69	0.74	0.0869 ± 0.0021	0.669 ± 0.041	0.0558 ± 0.0031	537 ± 12	444 ± 130
13.1	306	278	0.94	23.4	0.63	0.0887 ± 0.0020	0.746 ± 0.026	0.0610 ± 0.0016	548 ± 12	639 ± 58
16.1	56	5	0.09	4.54	2.07	0.0921 ± 0.0027	0.702 ± 0.123	0.0553 ± 0.0095	568 ± 16	425 ± 380

Table 4 (*Continued*)

Spot	U (ppm)	Th (ppm)	Th/U	Pb* (ppm)	Common ^{206}Pb (%)	Isotopic ratios			Ages (Ma)	
						^{206}Pb/^{238}U	^{207}Pb/^{235}U	^{207}Pb/^{206}Pb	^{206}Pb/^{238}U	^{207}Pb/^{206}Pb
Brightly luminescent rim										
1.2	292	109	0.39	21.8	0.75	0.0865 ± 0.0022	0.678 ± 0.031	0.0569 ± 0.0021	535 ± 13	486 ± 82
14.1	198	51	0.27	13.4	0.69	0.0782 ± 0.0028	0.690 ± 0.046	0.0641 ± 0.0037	485 ± 17	743 ± 120
15.1	240	96	0.41	18.7	1.29	0.0897 ± 0.0024	0.755 ± 0.057	0.0610 ± 0.0043	554 ± 14	641 ± 150
Sample MN1-1 (mafic granulite)										
1.1	268	50	0.19	20.3	0.15	0.0881 ± 0.0019	0.710 ± 0.020	0.0585 ± 0.0010	544 ± 12	547 ± 37
1.2	222	48	0.23	17.0	0.00	0.0892 ± 0.0020	0.738 ± 0.022	0.0600 ± 0.0013	551 ± 12	603 ± 44
2.1	106	33	0.32	8.39	0.25	0.0917 ± 0.0021	0.673 ± 0.050	0.0532 ± 0.0037	566 ± 13	337 ± 160
3.1	258	32	0.13	19.4	0.20	0.0873 ± 0.0020	0.700 ± 0.024	0.0581 ± 0.0015	540 ± 12	535 ± 55
4.1	243	23	0.10	18.5	0.19	0.0885 ± 0.0019	0.678 ± 0.026	0.0556 ± 0.0017	547 ± 12	436 ± 70
5.1	249	62	0.26	18.7	0.14	0.0875 ± 0.0023	0.682 ± 0.028	0.0565 ± 0.0018	541 ± 14	473 ± 70
6.1	409	42	0.11	31.2	0.18	0.0887 ± 0.0020	0.711 ± 0.018	0.0582 ± 0.0009	548 ± 11	535 ± 33
7.1	182	105	0.60	13.0	0.16	0.0834 ± 0.0020	0.671 ± 0.025	0.0584 ± 0.0017	516 ± 12	543 ± 64
8.1	293	72	0.25	23.5	0.00	0.0933 ± 0.0021	0.774 ± 0.022	0.0602 ± 0.0010	575 ± 12	611 ± 36
9.1	194	25	0.14	14.9	0.20	0.0891 ± 0.0020	0.674 ± 0.030	0.0549 ± 0.0021	550 ± 12	408 ± 84
Sample MP1-7 (felsic orthogneiss)										
Oscillatory zoned core										
1.1	188	159	0.87	26.8	0.79	0.1644 ± 0.0039	1.586 ± 0.059	0.0700 ± 0.0019	981 ± 22	928 ± 56
2.1	176	138	0.81	22.6	1.27	0.1476 ± 0.0035	1.371 ± 0.052	0.0673 ± 0.0020	888 ± 20	849 ± 62
3.1	190	188	1.02	25.0	0.95	0.1517 ± 0.0037	1.469 ± 0.053	0.0702 ± 0.0019	910 ± 20	935 ± 55
3.2	961	617	0.66	120	0.20	0.1453 ± 0.0033	1.386 ± 0.035	0.0692 ± 0.0007	875 ± 19	904 ± 20
4.1	263	204	0.80	33.0	1.02	0.1445 ± 0.0035	1.347 ± 0.044	0.0676 ± 0.0016	870 ± 19	857 ± 48
5.1	206	165	0.83	29.0	0.84	0.1629 ± 0.0039	1.555 ± 0.056	0.0692 ± 0.0019	973 ± 22	906 ± 55
6.1	282	313	1.15	39.3	0.49	0.1617 ± 0.0039	1.565 ± 0.045	0.0702 ± 0.0011	966 ± 21	935 ± 33
7.1	241	235	1.01	30.4	0.89	0.1456 ± 0.0035	1.413 ± 0.044	0.0704 ± 0.0014	876 ± 19	939 ± 40
8.1	272	292	1.11	33.5	0.72	0.1423 ± 0.0033	1.377 ± 0.041	0.0702 ± 0.0013	858 ± 19	933 ± 39
9.1	312	254	0.84	40.2	0.76	0.1491 ± 0.0036	1.418 ± 0.043	0.0690 ± 0.0012	896 ± 20	899 ± 37
10.1	189	206	1.13	21.4	1.83	0.1295 ± 0.0032	1.227 ± 0.059	0.0687 ± 0.0028	785 ± 19	891 ± 84
11.1	327	241	0.76	44.3	0.46	0.1568 ± 0.0036	1.519 ± 0.046	0.0703 ± 0.0013	939 ± 20	936 ± 37
12.1	224	171	0.79	28.4	0.77	0.1465 ± 0.0035	1.395 ± 0.049	0.0691 ± 0.0018	881 ± 20	901 ± 54
13.1	226	165	0.75	30.1	0.72	0.1543 ± 0.0037	1.515 ± 0.045	0.0712 ± 0.0013	925 ± 21	964 ± 38
14.1	151	150	1.03	18.5	1.02	0.1407 ± 0.0034	1.365 ± 0.064	0.0704 ± 0.0029	848 ± 19	940 ± 84
24.1	109	178	1.68	12.7	1.81	0.1331 ± 0.0033	1.292 ± 0.065	0.0704 ± 0.0030	806 ± 19	940 ± 87
25.1	827	453	0.57	113	0.15	0.1590 ± 0.0037	1.514 ± 0.036	0.0691 ± 0.0004	951 ± 20	901 ± 13
Darkly luminescent rim										
6.2	1861	201	0.11	139	0.17	0.0868 ± 0.0020	0.693 ± 0.017	0.0579 ± 0.0004	536 ± 12	526 ± 16
15.1	1697	352	0.21	123	0.16	0.0844 ± 0.0019	0.681 ± 0.016	0.0585 ± 0.0005	522 ± 12	547 ± 17
16.1	1771	275	0.16	136	0.19	0.0889 ± 0.0020	0.713 ± 0.017	0.0581 ± 0.0004	549 ± 12	534 ± 17
17.1	1667	322	0.20	126	0.19	0.0880 ± 0.0020	0.704 ± 0.017	0.0580 ± 0.0004	544 ± 12	529 ± 16
18.1	1608	281	0.18	122	0.13	0.0885 ± 0.0020	0.710 ± 0.017	0.0582 ± 0.0004	547 ± 12	536 ± 15
19.1	1474	256	0.18	111	0.14	0.0875 ± 0.0020	0.704 ± 0.017	0.0583 ± 0.0004	541 ± 12	542 ± 16
20.1	1367	250	0.19	103	0.11	0.0874 ± 0.0020	0.700 ± 0.017	0.0581 ± 0.0004	540 ± 12	535 ± 16
20.2	1287	248	0.20	94.9	0.23	0.0857 ± 0.0020	0.687 ± 0.017	0.0582 ± 0.0005	530 ± 12	536 ± 19
21.1	1262	220	0.18	90.3	0.18	0.0832 ± 0.0019	0.667 ± 0.017	0.0582 ± 0.0005	515 ± 11	536 ± 19
22.1	1323	251	0.20	99.3	0.15	0.0873 ± 0.0020	0.692 ± 0.017	0.0575 ± 0.0005	540 ± 12	511 ± 21
23.1	1625	272	0.17	130	0.21	0.0928 ± 0.0021	0.744 ± 0.018	0.0582 ± 0.0004	572 ± 13	535 ± 17
Sample ZR1-1 (felsic orthogneiss)										
Oscillatory zoned core										
1.1	380	173	0.47	51.4	0.20	0.1570 ± 0.0033	1.462 ± 0.048	0.0676 ± 0.0017	940 ± 19	855 ± 51
2.1	233	127	0.56	30.9	0.44	0.1532 ± 0.0034	1.509 ± 0.062	0.0714 ± 0.0025	919 ± 19	969 ± 72
3.1	352	152	0.45	48.4	0.06	0.1598 ± 0.0035	1.553 ± 0.059	0.0705 ± 0.0022	956 ± 19	942 ± 63
4.1	267	111	0.43	33.9	0.27	0.1474 ± 0.0032	1.418 ± 0.048	0.0698 ± 0.0017	886 ± 18	922 ± 52
5.1	182	79	0.45	26.6	0.05	0.1698 ± 0.0037	1.657 ± 0.048	0.0708 ± 0.0013	1011 ± 21	951 ± 39

Table 4 (*Continued*)

Spot	U (ppm)	Th (ppm)	Th/U	Pb* (ppm)	Common ^{206}Pb (%)	Isotopic ratios			Ages (Ma)	
						^{206}Pb/^{238}U	^{207}Pb/^{235}U	^{207}Pb/^{206}Pb	^{206}Pb/^{238}U	^{207}Pb/^{206}Pb
6.1	147	155	1.09	15.9	1.84	0.1240 ± 0.0030	0.945 ± 0.087	0.0553 ± 0.0049	753 ± 17	423 ± 200
8.1	121	68	0.58	16.3	0.39	0.1555 ± 0.0036	1.500 ± 0.062	0.0700 ± 0.0023	932 ± 20	928 ± 68
11.1	209	91	0.45	27.7	0.00	0.1544 ± 0.0037	1.463 ± 0.053	0.0688 ± 0.0019	926 ± 20	891 ± 57
12.1	303	140	0.48	38.3	0.27	0.1469 ± 0.0034	1.373 ± 0.062	0.0678 ± 0.0026	884 ± 19	862 ± 81
13.1	1240	363	0.30	150	0.08	0.1403 ± 0.0029	1.367 ± 0.037	0.0706 ± 0.0011	847 ± 17	947 ± 33
14.1	740	295	0.41	85.2	0.24	0.1337 ± 0.0028	1.238 ± 0.032	0.0672 ± 0.0010	809 ± 16	843 ± 31
15.1	328	164	0.52	42.6	0.19	0.1506 ± 0.0033	1.431 ± 0.044	0.0690 ± 0.0015	904 ± 18	897 ± 46
Darkly luminescent rim										
7.1	1054	89	0.09	83.4	0.21	0.0919 ± 0.0019	0.737 ± 0.018	0.0581 ± 0.0007	567 ± 12	534 ± 27
9.1	791	209	0.27	56.7	0.08	0.0834 ± 0.0018	0.656 ± 0.016	0.0571 ± 0.0007	516 ± 11	496 ± 26
10.1	876	217	0.26	68.6	0.61	0.0905 ± 0.0020	0.709 ± 0.025	0.0568 ± 0.0015	559 ± 12	485 ± 60
16.1	746	227	0.31	60.1	0.18	0.0936 ± 0.0020	0.755 ± 0.021	0.0585 ± 0.0011	577 ± 12	549 ± 41
17.1	1698	539	0.33	118	0.20	0.0809 ± 0.0017	0.650 ± 0.015	0.0582 ± 0.0006	502 ± 10	537 ± 23

Pb* denotes radiogenic Pb. Common ^{206}Pb (%) represents the proportion of common ^{206}Pb in total ^{206}Pb measured. Common Pb was corrected using the measured ^{204}Pb. All uncertainties are 1σ.

to be inherited ages. Eleven additional core analyses yielded a concordant population (from 964 ± 49 to 855 ± 60 Ma), with a weighted mean ^{207}Pb/^{206}Pb age of 907 ± 21 Ma (MSWD = 0.56) (Fig. 8a). This age is interpreted as the emplacement age of the protolith of mafic granulites. The remaining oscillatory zoned cores show younger ages, which might have resulted from partial recrystallization during the Late Neoproterozoic/Cambrian metamorphism. The data for 9 brightly luminescent rims or individual grains are all concordant and tightly grouped, yielding a mean ^{206}Pb/^{238}U age of 545 ± 9 Ma (MSWD = 1.3). Their Th/U ratios range from 0.29 to 0.38. This age is taken to indicate the time of metamorphism.

Note that the Th/U ratios in all the metamorphic overgrown domains of zircon in the Grove Mountains (also see below) are higher than the typical values of metamorphic zircons (e.g., Williams and Claesson, 1987; Rubatto and Gebauer, 2000). The case is very similar to the metamorphic zircons from high-grade rocks in the Rauer Group and EAIS (Harley et al., 1998; Liu et al., 2007). The reason for this is unclear, but as Möller et al. (2003) argued, the relatively high Th/U ratios for such zircon domains may have resulted from the open system behaviour, breakdown of high Th/U minerals such as monazite, or competition with high U minerals during metamorphism. Therefore, the present high Th/U ratios cannot be simply regarded as the indicator of non-metamorphic origin.

6.1.2. Sample MP2-4: mafic granulite

Zircons from sample MP2-4 are colorless or pale yellow and rounded to prismatic in shape, with grain sizes ranging from 30 to 150 μm. The CL images reveal core–rim structures in most grains (Fig. 7c and d). However, the oscillatory bands of most cores have been thickened and blurred as a consequence of solid-state recrystallization during metamorphism. Like sample ZR1-2, the rims are brightly luminescent and show planar growth banding or fir-tree sector zoning, which is indicative of metamorphic origin (Vavra et al., 1996). Seventeen U–Pb analyses on 16 zircon grains revealed that most zircon cores have ^{206}Pb/^{238}U ages similar to the rims (Fig. 8b), suggesting a complete recrystallization for them. Eleven concordant ages for both cores and rims are concentrated between 577 ± 14 and 528 ± 14 Ma, with a mean of 549 ± 8 Ma (MSWD = 1.2). Th/U ratios for these domains are variable from 0.09 to 1.91. This age is interpreted as the metamorphic age of the mafic granulite. Five other cores show older ages and higher Th/U ratios (0.95–2.92). However, the oldest one has a ^{206}Pb/^{238}U age of 742 ± 18 Ma (spot 6.1), still much younger than the protolith ages of the other samples. Therefore, it is not likely to represent the emplacement age of the mafic granulite protolith.

6.1.3. Sample MN1-1: mafic granulite

Zircons from sample MN1-1 are colorless and rounded to prismatic, with 20–120 μm in length. All zircon grains have recrystallized and show planar and fir-tree sector zonation (Fig. 7e and f), indicating a metamorphic recrystallization or overgrowth. The ^{206}Pb/^{238}U ages obtained for 10 analyses on 9 zircon grains range from 575 ± 12 to 516 ± 12 Ma. Excluding the oldest (spot 8.1) and the youngest (spot 7.1) data points that

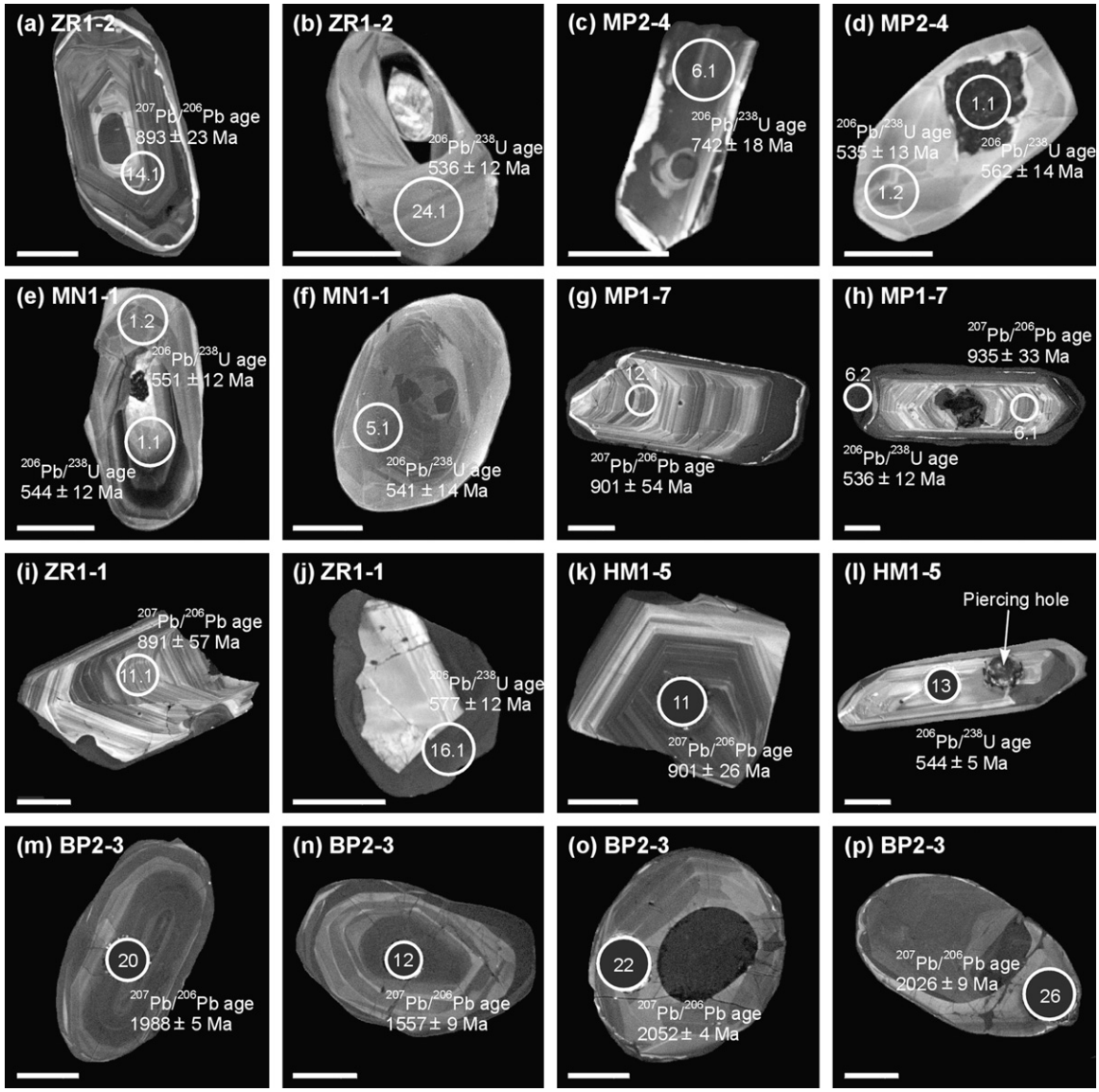

Fig. 7. Representative cathodoluminescence (CL) images of zircons from mafic granulites, felsic orthogneisses and paragneiss in the Grove Mountains. (a) Zircon from sample ZR1-2 showing a broad oscillatory zoned core and a gray overgrowth rim. A brighter band occurs on the outer border of the zoned core, indicating a recrystallization front. (b) Zircon from sample ZR1-2 showing bright, planar zoned domain with a brighter relict core. (c) Zircon from sample MP2-4 showing a broadly banded core and an irregular bright rim. (d) Zircon from sample MP2-4 showing a dark blurred core and bright, fir-tree sector zoned rim. (e) Zircon from sample MN1-1 showing planar and fir-tree sector zoning, indicating a solid-state recrystallization. (f) Zircon from sample MN1-1 showing typical fir-tree zonation. (g) Zircon from sample MP1-7 showing a fine-scaled oscillatory zoned core and a dark, discontinuous overgrowth rim. (h) Zircon from sample MP1-7 showing a fine-scaled oscillatory zoned core and a dark, thin overgrowth rim. (i) Zircon from sample ZR1-1 showing fine-scaled oscillatory zonation. (j) Zircon from sample ZR1-1 showing a bright core and a dark overgrowth rim. (k) Zircon from sample HM1-5 showing well-developed oscillatory zonation. (l) Zircon from sample HM1-5 showing a thick-banded core and a thin overgrowth rim. (m and n) Zircons from sample BP2-3 showing concentric planar zonation. (o) Zircon from sample BP2-3 showing a dark, homogeneous core and a bright, planar/sector zoned overgrowth rim. (p) Zircon from sample BP2-3 showing an oscillatory zoned core and a bright overgrowth rim. Circles with numbers are SHRIMP or LA-ICM-MS analytical spots with their identification numbers. Ages are given at 1σ (see Tables 4 and 5). Scale bars are 50 μm.

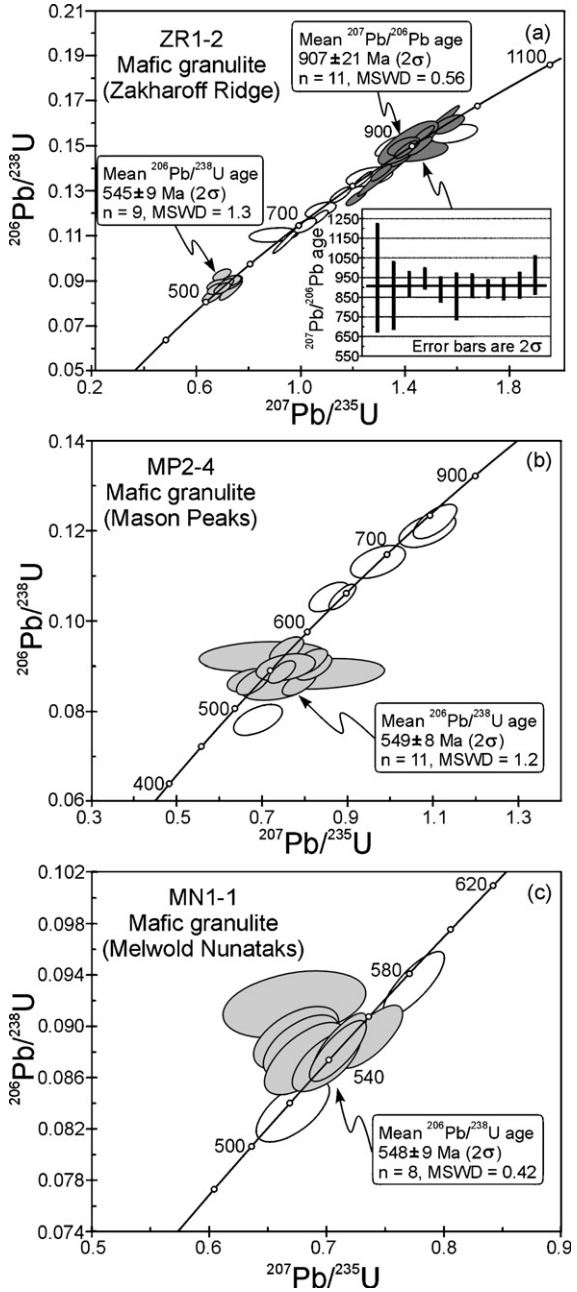

Fig. 8. SHRIMP zircon U–Pb concordia diagrams of mafic granulites from the Grove Mountains. (a) Sample ZR1-2 from Zakharoff Ridge. (b) Sample MP2-4 from Mason Peaks. (c) Sample MN1-1 from Melwold Nunataks.

may be resulted from earlier inheritance and later Pb loss, the 8 analyses are highly clustered with a mean age of 548 ± 9 Ma (MSWD = 0.42) (Fig. 8c). The Th/U ratios range from 0.10 to 0.60. The age is interpreted as the metamorphic age.

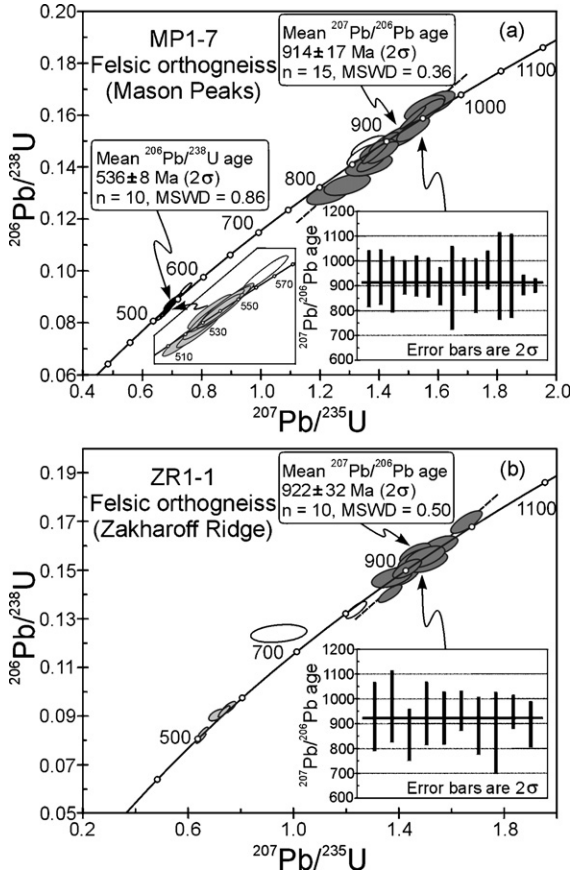

Fig. 9. SHRIMP zircon U–Pb concordia diagrams of felsic orthogneiss from the Grove Mountains. (a) Sample MP1-7 from Mason Peaks. (b) Sample ZR1-1 from Zakharoff Ridge.

6.1.4. *Sample MP1-7: felsic orthogneiss*

Zircons from sample MP1-7 are pale brown and prismatic, with 150–300 μm in length. They all show simple zoning patterns characterized by fine-scaled oscillatory zoned cores and darkly luminescent overgrowths (Fig. 7g and h). The overgrowths are usually thin and discontinuous, which are interpreted to have formed during metamorphism. Twenty-eight analyses on 21 zircon grains were performed on this sample. Except for spots 2.1 and 4.1 that show slightly young $^{207}Pb/^{206}Pb$ ages (849 ± 62 and 857 ± 48 Ma, respectively), the 15 core analyses display a discordant array and give $^{207}Pb/^{206}Pb$ ages ranging from 964 ± 38 to 891 ± 84 Ma (Fig. 9a), with a mean of 914 ± 17 Ma (MSWD = 0.36), which is identical to the upper intercept age of 914 ± 16 Ma. The Th/U ratios range from 0.57 to 1.68. We interpret the age of 914 Ma to be the protolith emplacement age. Apart from a reversely discordant spot 23.1, the $^{206}Pb/^{238}U$ ages obtained for 10 darkly luminescent overgrowths form a tight cluster (549 ± 12 to 515 ± 11 Ma) with a

mean of 536 ± 8 Ma (MSWD = 0.86) and Th/U ratios of 0.11–0.20. This age is interpreted to represent the timing of metamorphic recrystallization of felsic orthogneiss.

6.1.5. Sample ZR1-1: felsic orthogneiss

Zircons from sample ZR1-1 are pale yellow and ovoid to prismatic, with 100–200 μm in length. The CL images also display a fine-scaled oscillatory zoned core and a dark, homogeneous overgrowth rim (Fig. 7i and j). However, some zircons do not show any metamorphic overgrowths. The results of 17 U–Pb analyses on 17 zircon grains form two major populations (Fig. 9b). Among the oscillatory zoned cores, except for spots 6.1 and 14.1, all concordant spots produce a weighted mean $^{207}Pb/^{206}Pb$ age of 922 ± 32 Ma (MSWD = 0.50). Their Th/U ratios range from 0.30 to 0.58. This age is interpreted as the emplacement age of granitic protolith. The two exceptions showing younger ages probably reflect a Pb loss triggered by the later metamorphism. The data of five dark rims are scattered, yielding $^{206}Pb/^{238}U$ ages of 577 ± 12 to 502 ± 10 Ma, with Th/U ratios ranging from 0.09 to 0.33. The older age of 577 Ma might be resulted from a "contamination" by the oscillatory zoned cores because the analyzed rim is very small. The age is probably meaningless. However, the growth of new zircon rim strongly suggests that these ages are responsive to the Late Neoproterozoic/Cambrian metamorphic recrystallization.

6.2. LA-ICP-MS results

A felsic orthogneiss (sample HM1-5) and a paragneiss (sample BP2-3) were chosen for LA-ICP-MS U–Pb zircon analyses. The analytical data are listed in Table 5.

6.2.1. Sample HM1-5: felsic orthogneiss

Zircons from sample HM1-5 are euhedral and long prismatic, with 80–200 μm in length and a length to width ratio of 1.5–3.0. All zircon grains exhibit well-developed oscillatory zoning, but some oscillatory bands, particularly those on the zircon rims, have been thickened or blurred during late recrystallization (Fig. 7k and l). Only a few grains are observed to have a narrow, discontinuous overgrowth rim. Twenty-three analyses were carried out on zircon cores. Except for spot 13, 22 analyses give $^{207}Pb/^{206}Pb$ ages ranging from 1082 ± 90 to 823 ± 111 Ma (Fig. 10a), with Th/U ratios of 0.35–0.93. Excluding two younger (spots 5 and 17) and three older (spots 10, 15 and 22) data points that may be resulted from later Pb loss and earlier inheritance, respectively, the remaining 17 analyses define a discordant array with an upper intercept

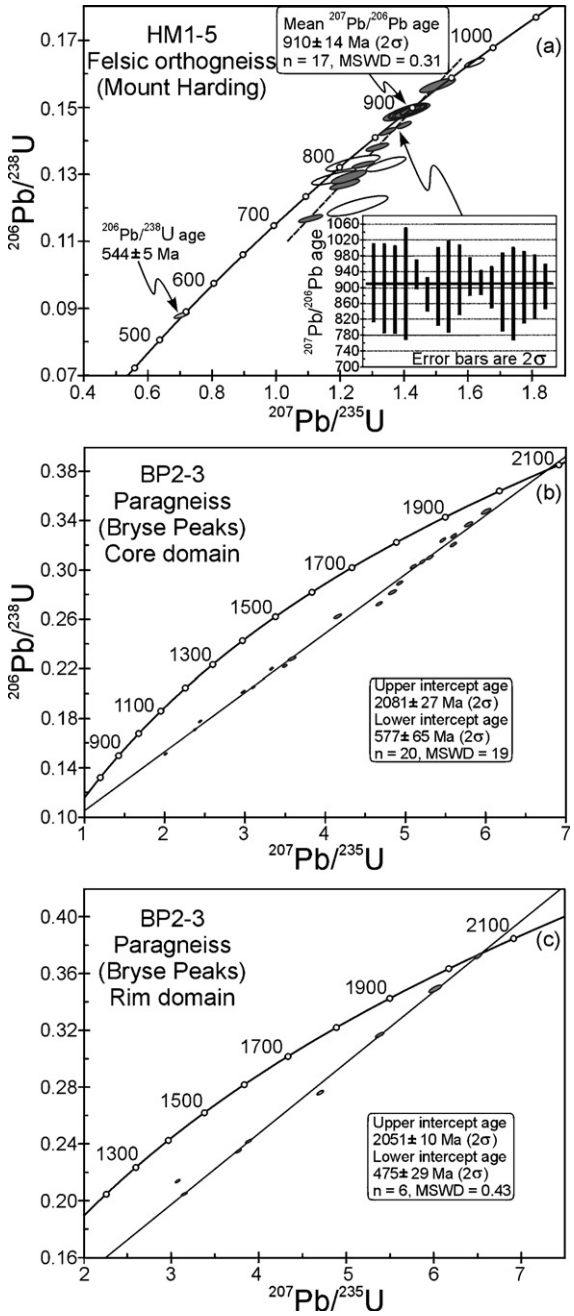

Fig. 10. LA-ICP-MS zircon U–Pb concordia diagrams of felsic orthogneiss and paragneiss from the Grove Mountains. (a) Felsic orthogneiss (sample HM1-5) from Mount Harding. (b) Zircon core domain in paragneiss (sample BP2-3) from Bryse Peaks. (c) Zircon rim domain in paragneiss (sample BP2-3) from Bryse Peaks.

age of 911 ± 20 Ma, which is identical within error to the weighted mean $^{207}Pb/^{206}Pb$ age of 910 ± 14 Ma (MSWD = 0.31) obtained for the same analyses. Thus, this age is considered to be the best estimate of the emplacement age of the protolith. The youngest spot 13

Table 5
LA-ICP-MS U–Pb analyses of zircons for felsic orthogneiss and paragneiss from the Grove Mountains

Spot	Th/U	Isotopic ratios			Ages (Ma)		
		$^{206}Pb/^{238}U$	$^{207}Pb/^{235}U$	$^{207}Pb/^{206}Pb$	$^{206}Pb/^{238}U$	$^{207}Pb/^{235}U$	$^{207}Pb/^{206}Pb$
Sample HM1-5 (felsic orthogneiss)							
1	0.93	0.1328 ± 0.0009	1.272 ± 0.029	0.0695 ± 0.0016	804 ± 5	833 ± 13	913 ± 49
2	0.71	0.1488 ± 0.0020	1.416 ± 0.053	0.0690 ± 0.0027	894 ± 11	896 ± 22	898 ± 56
3	0.60	0.1292 ± 0.0016	1.227 ± 0.045	0.0689 ± 0.0027	783 ± 9	813 ± 21	895 ± 55
4	0.40	0.1447 ± 0.0009	1.401 ± 0.019	0.0702 ± 0.0011	871 ± 5	889 ± 8	934 ± 18
5	0.58	0.1290 ± 0.0017	1.183 ± 0.059	0.0665 ± 0.0035	782 ± 10	793 ± 28	823 ± 111
6	0.49	0.1381 ± 0.0010	1.316 ± 0.029	0.0691 ± 0.0016	834 ± 6	853 ± 13	903 ± 49
7	0.35	0.1270 ± 0.0012	1.215 ± 0.038	0.0694 ± 0.0023	771 ± 7	808 ± 18	910 ± 70
8	0.54	0.1428 ± 0.0009	1.348 ± 0.021	0.0685 ± 0.0012	860 ± 5	867 ± 9	883 ± 21
9	0.88	0.1565 ± 0.0017	1.504 ± 0.046	0.0697 ± 0.0022	937 ± 10	932 ± 19	920 ± 44
10	0.53	0.1206 ± 0.0025	1.255 ± 0.077	0.0755 ± 0.0048	734 ± 14	826 ± 35	1082 ± 90
11	0.38	0.1492 ± 0.0011	1.421 ± 0.026	0.0691 ± 0.0014	897 ± 6	898 ± 11	901 ± 26
12	0.68	0.1491 ± 0.0017	1.412 ± 0.047	0.0687 ± 0.0024	896 ± 10	894 ± 20	889 ± 49
13	1.11	0.0880 ± 0.0008	0.705 ± 0.020	0.0581 ± 0.0017	544 ± 5	542 ± 12	534 ± 46
14	0.53	0.1487 ± 0.0015	1.417 ± 0.039	0.0692 ± 0.0020	894 ± 8	896 ± 16	903 ± 40
15	0.93	0.1330 ± 0.0018	1.344 ± 0.051	0.0733 ± 0.0029	805 ± 10	865 ± 22	1022 ± 55
16	0.52	0.1168 ± 0.0009	1.108 ± 0.031	0.0688 ± 0.0020	712 ± 5	757 ± 15	893 ± 62
17	0.61	0.1333 ± 0.0019	1.241 ± 0.069	0.0675 ± 0.0039	807 ± 11	819 ± 31	854 ± 123
18	0.91	0.1493 ± 0.0011	1.440 ± 0.025	0.0700 ± 0.0014	897 ± 6	906 ± 10	928 ± 24
19	0.58	0.1499 ± 0.0008	1.436 ± 0.016	0.0695 ± 0.0010	900 ± 5	904 ± 7	913 ± 15
20	0.51	0.1484 ± 0.0020	1.402 ± 0.055	0.0685 ± 0.0028	892 ± 11	890 ± 23	885 ± 58
21	0.52	0.1490 ± 0.0016	1.418 ± 0.043	0.0691 ± 0.0022	895 ± 9	897 ± 18	901 ± 45
22	0.45	0.1633 ± 0.0011	1.620 ± 0.025	0.0720 ± 0.0013	975 ± 6	978 ± 10	985 ± 21
23	0.70	0.1491 ± 0.0012	1.421 ± 0.028	0.0692 ± 0.0015	896 ± 6	898 ± 12	903 ± 28
Sample BP2-3 (paragneiss)							
Thickened oscillatory/planar zoned core							
1	0.14	0.3067 ± 0.0014	5.213 ± 0.030	0.1233 ± 0.0013	1724 ± 7	1855 ± 5	2005 ± 5
2	0.28	0.2280 ± 0.0014	3.585 ± 0.042	0.1140 ± 0.0015	1324 ± 7	1546 ± 9	1865 ± 24
3	0.03	0.3206 ± 0.0015	5.600 ± 0.032	0.1267 ± 0.0013	1793 ± 7	1916 ± 5	2053 ± 5
4	0.09	0.3276 ± 0.0015	5.600 ± 0.030	0.1240 ± 0.0013	1827 ± 7	1916 ± 5	2015 ± 4
5	0.10	0.2016 ± 0.0010	2.978 ± 0.020	0.1072 ± 0.0012	1184 ± 5	1402 ± 5	1752 ± 6
6	0.12	0.2820 ± 0.0015	4.839 ± 0.039	0.1245 ± 0.0012	1601 ± 8	1792 ± 7	2021 ± 18
7	0.06	0.3475 ± 0.0019	6.006 ± 0.048	0.1254 ± 0.0015	1923 ± 9	1977 ± 7	2034 ± 7
8	0.03	0.1710 ± 0.0008	2.377 ± 0.017	0.1009 ± 0.0011	1018 ± 5	1236 ± 5	1640 ± 6
9	0.02	0.3242 ± 0.0014	5.464 ± 0.029	0.1223 ± 0.0008	1810 ± 7	1895 ± 4	1989 ± 12
10	0.03	0.2199 ± 0.0010	3.331 ± 0.019	0.1098 ± 0.0008	1281 ± 5	1488 ± 5	1797 ± 14
11	0.45	0.3370 ± 0.0016	5.788 ± 0.042	0.1246 ± 0.0011	1872 ± 8	1945 ± 6	2022 ± 16
12	0.09	0.1513 ± 0.0008	2.013 ± 0.017	0.0965 ± 0.0012	908 ± 4	1120 ± 6	1557 ± 9
13	0.06	0.2726 ± 0.0014	4.674 ± 0.033	0.1244 ± 0.0011	1554 ± 7	1763 ± 6	2020 ± 16
14	0.19	0.3102 ± 0.0014	5.306 ± 0.034	0.1241 ± 0.0010	1742 ± 7	1870 ± 5	2016 ± 14
15	0.10	0.1777 ± 0.0009	2.443 ± 0.018	0.0997 ± 0.0012	1055 ± 5	1255 ± 5	1618 ± 7
16	0.17	0.2625 ± 0.0015	4.158 ± 0.040	0.1449 ± 0.0013	1502 ± 7	1666 ± 8	1878 ± 20
17	0.02	0.2053 ± 0.0009	3.103 ± 0.019	0.1096 ± 0.0008	1204 ± 5	1434 ± 5	1793 ± 14
18	0.15	0.2223 ± 0.0011	3.497 ± 0.025	0.1141 ± 0.0010	1294 ± 6	1527 ± 6	1866 ± 16
19	0.05	0.2894 ± 0.0014	4.928 ± 0.031	0.1235 ± 0.0010	1638 ± 7	1807 ± 5	2008 ± 14
20	0.04	0.3027 ± 0.0014	5.098 ± 0.031	0.1221 ± 0.0013	1704 ± 7	1836 ± 5	1988 ± 5
Brightly luminescent rim							
21	0.50	0.3170 ± 0.0014	5.382 ± 0.039	0.1231 ± 0.0011	1775 ± 7	1882 ± 6	2002 ± 16
22	0.65	0.3726 ± 0.0016	6.508 ± 0.033	0.1266 ± 0.0014	2042 ± 7	2047 ± 4	2052 ± 4
23	0.43	0.2351 ± 0.0010	3.770 ± 0.027	0.1163 ± 0.0010	1361 ± 5	1586 ± 6	1900 ± 15
24	0.27	0.2139 ± 0.0009	3.076 ± 0.023	0.1043 ± 0.0009	1249 ± 5	1427 ± 6	1702 ± 16
25	0.47	0.2419 ± 0.0011	3.883 ± 0.028	0.1165 ± 0.0010	1396 ± 5	1610 ± 6	1902 ± 16
26	0.43	0.3495 ± 0.0021	6.016 ± 0.059	0.1248 ± 0.0017	1932 ± 10	1978 ± 9	2026 ± 9
27	0.44	0.2760 ± 0.0013	4.702 ± 0.030	0.1235 ± 0.0014	1571 ± 6	1768 ± 5	2007 ± 6
28	0.39	0.2047 ± 0.0010	3.150 ± 0.028	0.1116 ± 0.0011	1201 ± 5	1445 ± 7	1826 ± 18

Common Pb was corrected using the method of Anderson (2002). All uncertainties are 1σ.

is almost concordant and gives a $^{206}Pb/^{238}U$ apparent age of 544 ± 5 Ma, which is also in agreement with the metamorphic age inferred from mafic granulites. The strongly thickened bands on this zircon support their formation by metamorphic solid-state recrystallization.

6.2.2. Sample BP2-3: paragneiss

Zircons from sample BP2-3 are all rounded or ovoid, with grain sizes ranging from 50 to 200 μm. Most zircon grains have low CL response and show thickened oscillatory or concentric planar zoning (Fig. 7m–p) that are interpreted as recrystallization of magmatic zircons. Some grains have a thick and brightly luminescent rim, which shows planar growth banding and sector zoning, probably of metamorphic origin. Considering their well-rounded features and sedimentary derivation, we interpret these zircons to be of detrital origin. The irregular, darkly luminescent rims can be observed on several detrital grains. They are assumed to have formed during the Late Neoproterozoic/Cambrian metamorphism, but it is too narrow (<10 μm) to be analyzed. Twenty-eight U–Pb analyses reveal that there is no clear age difference between zircon cores and bright rims; they all show different degrees of discordancy due to variable radiogenic Pb loss. The data points fall on or near a discordia with an upper intercept age of 2075 ± 23 Ma and a lower intercept age of 569 ± 59 Ma. If calculated separately, 20 core analyses yield an upper intercept age of 2081 ± 27 Ma and a lower intercept age of 577 ± 65 Ma (Fig. 10b). Their Th/U ratios are mostly low, ranging from 0.02 to 0.19 (except for spots 2 and 11 with Th/U ratios of 0.28 and 0.45, respectively). By comparison, 6 rim analyses (excluding spots 24 and 27) yield an upper intercept age of 2051 ± 10 Ma and a lower intercept age of 475 ± 29 Ma (Fig. 10c), with Th/U ratios of 0.27–0.65. In fact, spot 22 is nearly concordant, giving a $^{207}Pb/^{206}Pb$ age of 2052 ± 4 Ma, which is identical to the above upper intercept age. Based on the CL characteristics, the age of ca. 2050 Ma is interpreted to represent an Early Paleoproterozoic metamorphic event. The age similarity between zircon cores and rims may further suggest that the magmatic cores have strongly recrystallized during metamorphism. It is important to note that no record of Early Neoproterozoic age (ca. 990–900 Ma) was found in zircons from this sample.

7. Discussion

7.1. A massive igneous intrusion at ca. 920–910 Ma

Multiple stages of growth and recrystallization of zircons are commonly used to trace the tectonothermal history of a polymetamorphic terrane. Even in a high-temperature granulite facies condition, zircons or individual zircon domains of earlier generations might have escaped dissolution or recrystallization during metamorphism. In such a case, the ages of earlier thermal events could be obtained for well-preserved zircon domains (e.g., Vavra et al., 1996, 1999). For high-grade rocks in the Grove Mountains, zircon cores from felsic orthogneisses and some mafic granulites are shown to have well preserved oscillatory zoning of magmatic origin, hence the emplacement age of mafic–felsic magma can be determined. In the present study, five samples (including sample MN1-5 previously dated by Zhao et al., 2000) collected from different localities over an extensive area yielded tightly grouped ages of ca. 920–910 Ma. Apparently, the ca. 920–910 Ma magmatic intrusion in this area is very voluminous, which is different from the weak magmatic activity occurring at this time (ca. 910–900 Ma) in the Rayner Complex (Boger et al., 2000; Carson et al., 2000).

It has been established that the Early Neoproterozoic high-grade metamorphism took place at ca. 990–930 Ma in the Rayner Complex and Søstrene Island (Hensen and Zhou, 1995; Kinny et al., 1997; Boger et al., 2000; Kelly et al., 2002). Therefore, the mafic–felsic intrusion in the period of ca. 920–910 Ma in the Grove Mountains probably represents an episode of a widespread Early Neoproterozoic post-orogenic magmatism. This appears to be supported by the geochemical characteristics of mafic granulites and felsic orthogneisses. As mentioned previously, HFS trace element characteristics indicate a subalkaline affinity of continental intraplate basalts for mafic granulites. All the felsic orthogneisses share the same characteristics as A_2-type granites, whilst A_2-type granite magmatism is generally a diagnostic feature of post-collisional or post-orogenic extensional environments (Eby, 1992). In the tectonic discrimination diagram of Pearce et al. (1984), most felsic orthogneisses fall in the WPG field. As pointed out by Förster et al. (1997), late- or post-collisional granites in a continent–continent collision setting tend to produce a WPG affinity. In fact, underplating of mantle-derived mafic magma, as a consequence of lithospheric delamination and asthenospheric upwelling, often occurs during post-collisional extension of an orogen. Therefore, voluminous magma intrusion in an orogen often took place at this late stage. Taking into account the bimodal characteristics of mafic–felsic intrusives in the Grove Mountains, we infer that this intense magmatism may mark the termination of the Early Neoproterozoic orogenesis.

The near-zero $\varepsilon_{Nd}(T)$ values (+0.8 to −0.7) for the low-Ti granulites suggest that the primary mafic magma was derived from partial melting of a weakly enriched subcontinental lithospheric mantle. Sample E2-2, which shows the highest Mg# and La/Nb and slightly positive Eu and Sr anomalies, may represent the least evolved magma. The positive correlation between TiO_2 and FeO^t/MgO ratios for the rocks could be interpreted by fractional crystallization. The enrichment of Ti and P in high-Ti granulites is likely resulted from the cumulation of Fe–Ti oxides and apatite at elevated oxygen fugacity during the magma evolution. However, the negative correlation between TiO_2 and $\varepsilon_{Nd}(T)$ values and the positive correlation between TiO_2 and La/Nb ratios may also reflect crustal contamination during fractional crystallization of the magma.

Relative to the Mesoproterozoic–Neoproterozoic granitoids from the Prydz Bay and the Rayner Complex (Hensen and Zhou, 1995; Young et al., 1997; Zhao et al., 1997), the dominant felsic orthogneisses from the Grove Mountains have higher $\varepsilon_{Nd}(T)$ values of −0.7 to −3.5 and younger T_{DM} of 1.76–1.65 Ga. This suggests that the felsic magma in the Grove Mountains contains a significant proportion of the mantle component and does not share the same source regions with granitoids from the Prydz Bay and the Rayner Complex. Owing to the geochemical characteristics of A_2-type granites, felsic orthogneisses from the Grove Mountains were likely formed by high-temperature partial melting of continental crust of tonalitic-granodioritic composition (Eby, 1992). The heat responsible for partial melting may have come from the basaltic underplating during crustal extension. However, two samples with $\varepsilon_{Nd}(T)$ values (−10.4 to −10.6) and T_{DM} (2.46–2.27 Ga), significantly different from the other felsic orthogneisses, argue for a heterogeneity in their source region and existence of an Early Paleoproterozoic crust in the area.

7.2. A single metamorphic event at ca. 550–535 Ma

It is very important to note that there is no evidence for Early Neoproterozoic metamorphic zircon growth on primary magmatic zircon cores from the mafic and felsic rocks of the Grove Mountains. Although some zircon cores yield ages slightly younger than ca. 910 Ma, the preservation of oscillatory zoning suggests that Pb loss in such zircon domains might have resulted from partial recrystallization during the Late Neoproterozoic/Cambrian metamorphism. Furthermore, the Early Paleoproterozoic detrital zircons from paragneiss have not recorded such an event either. Consequently, we may conclude that the Early Neoproterozoic metamorphic event was absent in the Grove Mountains, and that all the mineral assemblages and textures recorded in the high-grade rocks from this area were produced during a single Late Neoproterozoic/Cambrian metamorphic episode.

On the basis of U–Pb zircon and monazite ages of 535–527 Ma obtained for anatectic leucogneisses (Fitzsimons et al., 1997), Sm–Nd whole rock-garnet isochron ages of 517–490 Ma for para- and orthogneisses (Hensen and Zhou, 1995) and U–Pb zircon ages of 516–514 Ma for granites (Carson et al., 1996), the peak metamorphism in the Prydz Bay area was considered to have occurred at ca. 535–530 Ma (Fitzsimons, 2003; Harley, 2003; Zhao et al., 2003). The present study reveals that the zircon recrystallization in the rocks of the Grove Mountains took place from 549 to 536 Ma. Particularly for zircons from mafic granulites, the overgrowth ages are tightly grouped at 549–545 Ma, which is identical to the emplacement age (547 ± 1 Ma) of the charnockite obtained by ID-TIMS analysis (Liu et al., 2006). Therefore, we infer that the high-grade metamorphism of the Grove Mountains took place at least at ca. 550 Ma. It seems that the formation age of the Prydz Belt is roughly contemporaneous with the late collisional stage in the East African Orogen (Kröner and Williams, 1993; Paquette et al., 1994; Shiraishi et al., 1994; Goscombe et al., 1998; Jacobs et al., 2003; Fitzsimons and Hulscher, 2005).

7.3. Regional correlations and tectonic implications

We have established that the protoliths of mafic granulites and felsic orthogneisses were formed at ca. 920–910 Ma. We have also observed that some metasedimentary rocks contain detrital zircons with metamorphic age of ca. 2050 Ma. These metaigneous and metasedimentary rocks constitute the Early Neoproterozoic basement terrane in the Grove Mountains. The detrital zircon age is in good agreement with a metamorphic age of 2065 ± 23 Ma obtained for an augen gneiss from the Lambert Terrane of SPCM (Mikhalsky et al., 2006), suggesting that the materials of the paragneiss in the Grove Mountains could have come from an unknown Early Paleoproterozoic orogen probably related to the Lambert Terrane. The depositional age of the materials are not well constrained, but the absence of detrital zircons of ca. 920–910 Ma in the rocks suggests that the deposition took place before the emplacement of the Early Neoproterozoic intrusives. Considering the isotopic compositions and geochronology of the major geological events, the basement terrane of the Grove Mountains can be distinguished from the other segments of the Prydz Belt, and from the southeastern part of the

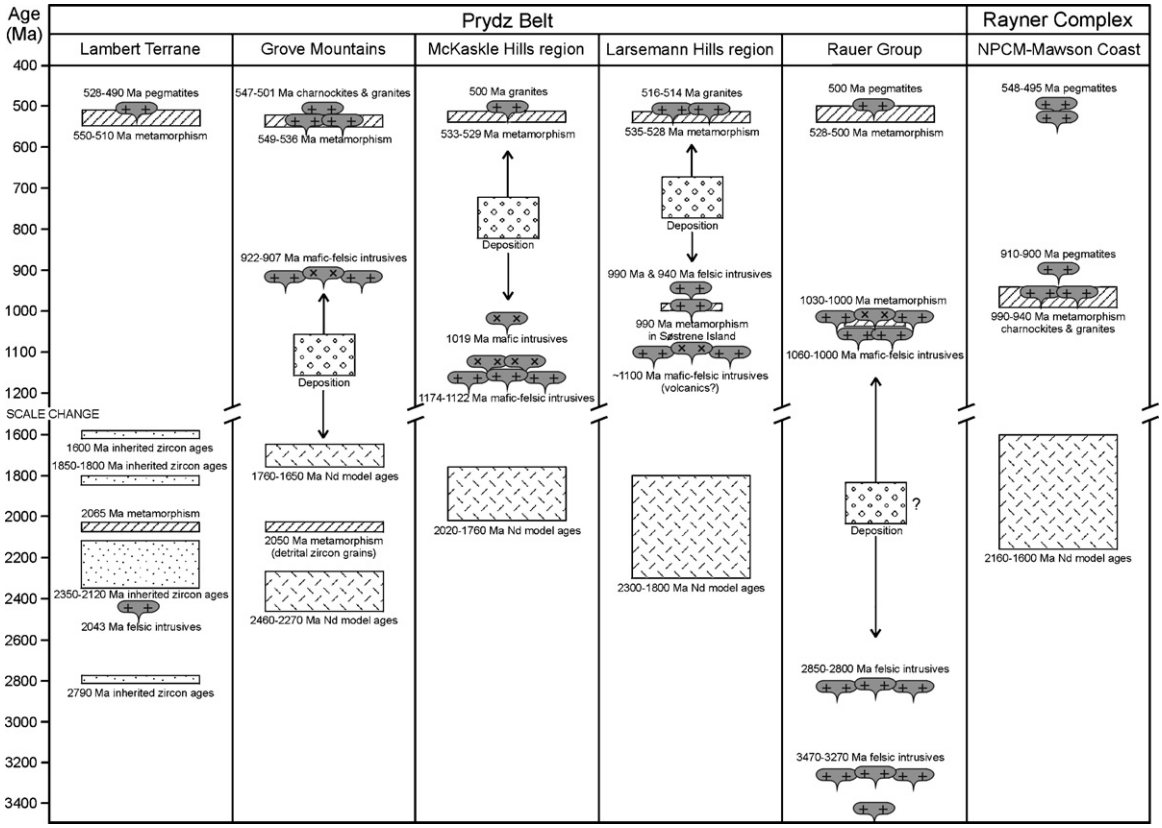

Fig. 11. Time–space diagram for main segments of the Prydz Belt and adjacent northern Prince Charles Mountains–Mawson Coast area. *References*: the Lambert Terrane from Boger et al. (2001) and Mikhalsky et al. (2006); the Grove Mountains from Liu et al. (2006) and this study; the McKaskle Hills region (including the Landing Bluff) from Tingey (1991) and Liu et al. (2007); the Larsemann Hills region (including the Bolingen Islands and Brattstrand Bluffs) from Hensen and Zhou (1995), Zhao et al. (1995, 2003), Carson et al. (1996), Zhang et al. (1996), Fitzsimons et al. (1997) and Y. Wang et al. (2003); the Rauer Group from Kinny et al. (1993), Harley et al. (1998) and Kelsey et al. (2003); the NPCM–Mawson Coast area from Young and Black (1991), Manton et al. (1992), Young et al. (1997), Zhao et al. (1997), Carson et al. (2000) and Boger et al. (2000, 2002).

Rayner Complex (i.e., the NPCM–Mawson Coast area) as schematically shown in Fig. 11. Indeed, even within the Prydz Belt, the different segments, as revealed in the Lambert Terrane, the Grove Mountains, the McKaskle Hills region, the Larsemann Hills region and the Rauer Group, also have different Precambrian tectonic histories (see Fig. 11). Therefore, the Prydz Belt is likely to represent a collage of multiple basement terranes.

The present study precludes an Early Neoproterozoic metamorphic event in the Grove Mountains. In fact, this event is only documented in a large mafic granulite body from Søstrene Island (Hensen and Zhou, 1995) and probably in some rocks from the Rauer Group (Kinny et al., 1993), whereas the more widespread rocks in the Prydz Belt have only undergone a single Late Neoproterozoic/Cambrian metamorphic cycle. Particularly in felsic orthogneisses from the McKaskle Hills of EAIS, CL images of zircons revealed that the Cambrian metamorphic zircons grew directly on the Mesoproterozoic magmatic zircon domains (Liu et al., 2007). Therefore, the effect of the Early Neoproterozoic metamorphism in the whole Prydz Belt is very limited. This indicates that the different basement terranes in the Prydz Belt were probably not juxtaposed during the Early Neoproterozoic orogenesis. Consequently, the intracontinental reworking model for the Late Neoproterozoic/Cambrian tectonism, as preferred by some workers (Yoshida, 1995; Wilson et al., 1997; Yoshida et al., 2003), is not favored. Instead, the fact that all the basement terranes have suffered from the same Late Neoproterozoic/Cambrian high-grade metamorphism and showed the same clockwise metamorphic *P–T* paths (Thost et al., 1994; Fitzsimons, 1996; Carson et al., 1997; Boger and Wilson, 2005; Liu et al., 2006, 2007) strongly supports the idea that the Prydz Belt represents a collisional orogen resulted in the final phase

of the Gondwana assembly during the Late Neoproterozoic/Cambrian period (e.g., Fitzsimons, 2000, 2003; Boger et al., 2001; Zhao et al., 2003).

8. Conclusions

The present geochemical and geochronological study leads to the following conclusions:

(1) A detailed zircon geochronology on mafic granulites and felsic orthogneisses from the Grove Mountains reveals an important mafic and felsic magmatism at ca. 920–910 Ma. The occurrence of coeval intrusives in the Rayner Complex and the geochemical signature of mafic granulites and felsic orthogneisses suggest that this igneous event was part of a widespread episode of Early Neoproterozoic post-orogenic magmatism.
(2) Geochemical and Nd isotopic characteristics indicate that the primary magma of mafic granulites was likely generated by partial melting of a weakly enriched subcontinental lithospheric mantle. Fractional crystallization, accompanied by minor crustal contamination, produced the protoliths of low- to high-Ti granulites. The felsic orthogneisses have an affinity of A_2-type granites; they were probably derived from high-temperature partial melting of tonalitic-granodioritic rocks triggered by the underplating of mantle-derived mafic magma during post-orogenic extension.
(3) The Early Neoproterozoic emplacement ages of both mafic granulites and felsic orthogneisses and the Late Paleoproterozoic Nd model ages (1.76–1.65 Ga) of most felsic orthogneisses suggest that the Grove Mountains area is different from the southern Prydz Bay-eastern Amery Ice Shelf Mesoproterozoic basement. Moreover, the metamorphic age of ca. 2050 Ma obtained for detrital zircons from a paragneiss may indicate an Early Paleoproterozoic orogeny occurring in the area. Therefore, the Grove Mountains may represent a distinct basement terrane in the Prydz Belt.
(4) The available data indicate that the Prydz Belt is a collage of basement terranes of distinct tectonic evolution. However, all the basement terranes have suffered from the same Late Neoproterozoic/Cambrian high-grade metamorphic event. This supports the suggestion that the Prydz Belt represents a collisional orogen that resulted in the final phase of the Gondwana assembly during the Late Neoproterozoic/Cambrian period.

Acknowledgements

We would like to thank J. Li and D. Huo for assistance during field work and X.-H. Li for fruitful discussions. Yuruo Shi and Laicheng Miao kindly assisted in the SHRIMP U–Pb zircon analyses and Wenliang Xu in the LA-ICP-MS analyses. I. C. W. Fitzsimons and C. J. Carson are thanked for their detailed and critical reviews, which greatly improved the manuscript. The field work was carried out during the 1998–1999 Chinese National Antarctic Research Expedition. Logistic support by the Antarctic Administration of China and financial support by the National Natural Science Foundation of China (No. 40372046), Geological Investigation Project of China Geological Survey (1212010511505) and Programme of Young Scientists of the Ministry of Land and Resources are gratefully acknowledged. Xiaochun Liu benefited from a one-year stay in the Department of Geosciences, National Taiwan University, and a three-month visit in Department of Earth Sciences, The University of Hong Kong. Bor-Ming Jahn acknowledges the financial support of the National Science Council of Taiwan through grants NSC-92-2811-M-002-056 and NSC-93-2116-M-002-006.

References

Anderson, T., 2002. Correction of common lead in U–Pb analyses that do not report ^{204}Pb. Chem. Geol. 192, 59–79.

Beliatsky, B.V., Laiba, A.A., Mikhalsky, E.V., 1994. U–Pb zircon age of the metavolcanic rocks of Fisher Massif (Prince Charles Mountains, East Antarctica). Antarct. Sci. 6, 355–358.

Black, L.P., Kamo, S.L., Allen, C.M., Aleinikoff, J.N., Davis, D.W., Korsch, R.J., Foudoulis, C., 2003. TEMORA 1: a new standard for Phanerozoic U–Pb geochronology. Chem. Geol. 200, 155–170.

Boger, S.D., Carson, C.J., Wilson, C.J.L., Fanning, C.M., 2000. Neoproterozoic deformation in the northern Prince Charles Mountains, East Antarctica: evidence for a single protracted orogenic event. Precambrian Res. 104, 1–24.

Boger, S.D., Wilson, C.J.L., Fanning, C.M., 2001. Early Paleozoic tectonism within the East Antarctic craton: the final suture between east and west Gondwana? Geology 29, 463–466.

Boger, S.D., Carson, C.J., Fanning, C.M., Hergt, J.M., Wilson, C.J.L., Woodhead, J.D., 2002. Pan-African intraplate deformation in the northern Prince Charles Mountains, East Antarctica. Earth Planet. Sci. Lett. 195, 195–210.

Boger, S.D., Wilson, C.J.L., 2005. Early Cambrian crustal shortening and a clockwise P–T–t path from the southern Prince Charles Mountains, East Antarctica: implications for the formation of Gondwana. J. Metamorph. Geol. 23, 603–623.

Carson, C.J., Dirks, P.G.H.M., Hand, M., Sims, J.P., Wilson, C.J.L., 1995. Compressional and extensional tectonics in low-medium pressure granulites from the Larsemann Hills, East Antarctica. Geol. Mag. 132, 151–170.

Carson, C.J., Fanning, C.M., Wilson, C.J.L., 1996. Timing of the Progress Granite, Larsemann Hills: evidence for Early Palaeozoic

orogenesis within the East Antarctica Shield and implications for Gondwana assembly. Aust. J. Earth Sci. 43, 539–553.

Carson, C.J., Powell, P., Wilson, C.J.L., Dirks, P.H.G.M., 1997. Partial melting during tectonic exhumation of a granulite terrane: an example from the Larsemann Hills, East Antarctica. J. Metamorph. Geol. 15, 105–126.

Carson, C.J., Boger, S.D., Fanning, C.M., Wilson, C.J.L., Thost, D.E., 2000. SHRIMP U–Pb geochronology from Mount Kirkby, northern Prince Charles Mountains, East Antarctica. Antarct. Sci. 12, 429–442.

Dirks, P.H.G.M., Wilson, C.J.L., 1995. Crustal evolution of the East Antarctic mobile belt in Prydz Bay: continental collision at 500 Ma? Precambrian Res. 75, 189–207.

Eby, G.N., 1992. Chemical subdivision of the A-type granitoids: petrogenesis and tectonic implications. Geology 20, 641–644.

Fitzsimons, I.C.W., 1996. Metapelitic migmatites from Brattstrand Bluffs, East Antarctica—metamorphism, melting and exhumation of the mid crust. J. Petrol. 37, 395–414.

Fitzsimons, I.C.W., 1997. The Brattstrand Paragneiss and the Søstrene Orthogneiss: a review of Pan-African metamorphism and Grenvillian relics in southern Prydz Bay. In: Ricci, C.A. (Ed.), The Antarctic Region: Geological Evolution and Processes. Terra Antarctica Publishers, Siena, pp. 121–130.

Fitzsimons, I.C.W., 2000. Grenville-age basement provinces in East Antarctica: evidence for three separate collisional orogens. Geology 28, 879–882.

Fitzsimons, I.C.W., 2003. Proterozoic basement provinces of southern and southwestern Australia, and their correlation with Antarctica. In: Yoshida, M., Windley, B., Dasgupta, S. (Eds.), Proterozoic East Gondwana: Supercontinent Assembly and Breakup, vol. 206. Geological Society, London, pp. 93–130 (special publication).

Fitzsimons, I.C.W., Harley, S.L., 1991. Geological relationships in high-grade gneisses of the Brattstrand Bluffs coastline, Prydz Bay, East Antarctica. Aust. J. Earth Sci. 38, 497–519.

Fitzsimons, I.C.W., Hulscher, B., 2005. Out of Africa: detrital zircon provenance of central Madagascar and Neoproterozoic terrane transfer across the Mozambique Ocean. Terra Nova 17, 224–235.

Fitzsimons, I.C.W., Kinny, P.D., Harley, S.L., 1997. Two stages of zircon and monazite growth in anatectic leucogneiss: SHRIMP constraints on the duration and intensity of Pan-African metamorphism in Prydz Bay, East Antarctica. Terra Nova 9, 47–51.

Förster, H.-J., Tischendorf, G., Trumbull, R.B., 1997. An evaluation of the Rb vs. (Y + Nb) discrimination diagram to infer tectonic setting of silicic igneous rocks. Lithos 40, 261–293.

Goscombe, B., Armstrong, R., Barton, J.M., 1998. Tectonometamorphic evolution of the Chewore inliers: partial re-equilibration of high-grade basement during the Pan-African orogeny. J. Petrol. 39, 1347–1384.

Harley, S.L., 2003. Archaean-Cambrian crustal development of East Antarctica: metamorphic characteristics and tectonic implications. In: Yoshida, M., Windley, B., Dasgupta, S. (Eds.), Proterozoic East Gondwana: Supercontinent Assembly and Breakup, vol. 206. Geological Society, London, pp. 203–230 (special publication).

Harley, S.L., Snape, I., Black, L.P., 1998. The early evolution of a layered metaigneous complex in the Rauer Group, East Antarctica: evidence for a distinct Archaean terrane. Precambrian Res. 89, 175–205.

Hensen, B.J., Zhou, B., 1995. A Pan-African granulite facies metamorphic episode in Prydz Bay, Antarctica: evidence from Sm–Nd garnet dating. Aust. J. Earth Sci. 42, 249–258.

Hoskin, P.W.O., Black, L.P., 2000. Metamorphic zircon formation by solid-state recrystallization of protolith igneous zircon. J. Metamorph. Geol. 18, 423–439.

Jacobs, J., Bauer, W., Fanning, C.M., 2003. Late Neoproterozoic/Early Palaeozoic events in central Dronning Maud Land and significance for the southern extension of the East African Orogen into East Antarctica. Precambrian Res. 126, 27–53.

Kelly, N.M., Clarke, G.L., Fanning, C.M., 2002. A two-stage evolution of the Neoproterozoic Rayner Structural Episode: new U–Pb sensitive high resolution ion microprobe constraints from the Oygarden Group, Kemp Land, East Antarctica. Precambrian Res. 111, 307–330.

Kelsey, D.E., Powell, R., Wilson, C.J.L., Steele, D.A., 2003. (Th + U)-Pb monazite ages from Al-Mg-rich metapelites, Rauer Group, East Antarctica. Contrib. Mineral. Petrol. 146, 326–340.

Kinny, P.D., Black, L.P., Sheraton, J.W., 1993. Zircon ages and the distribution of Archean and Proterozoic rocks in the Rauer Islands. Antarct. Sci. 5, 193–206.

Kinny, P.D., Black, L.P., Sheraton, J.W., 1997. Zircon U–Pb ages and geochemistry of igneous and metamorphic rocks in the northern Prince Charles Mountains, Antarctica. AGSO J. Aust. Geol. Geophys. 16, 637–654.

Kröner, A., Williams, I.S., 1993. Age of metamorphism in the high-grade rocks of Sri Lanka. J. Geol. 101, 513–521.

Liu, X.C., Zhao, Y., Liu, X.H., 2002. Geological aspects of the Grove Mountains, East Antarctica. Antarctica at the close of a millennium. In: Gamble, J.A., Skinner, D.N.B., Henrys, S. (Eds.), R. Soc. N. Z. Bull. 35, 161–166.

Liu, X.H., Zhao, Y., Liu, X.C., Yu, L., 2003. Geology of the Grove Mountains in East Antarctica – new evidence for the final suture of Gondwana Land. Sci. China (Ser. D) 46, 305–319.

Liu, X.C., Zhao, Z., Zhao, Y., Chen, J., Liu, X.H., 2003. Pyroxene exsolution in mafic granulites from the Grove Mountains, East Antarctica: constraints on the Pan-African metamorphic conditions. Eur. J. Mineral 15, 55–65.

Liu, X.C., Jahn, B.-M., Zhao, Y., Li, M., Li, H., Liu, X.H., 2006. Late Pan-African granitoids from the Grove Mountains, East Antarctica: age, origin and tectonic implications. Precambrian Res. 145, 131–154.

Liu, X.C., Zhao, Y., Zhao, G., Jian, P., Xu, G., 2007. Petrology and geochronology of granulites from the McKaskle Hills, eastern Amery Ice Shelf, Antarctica, and implications for the evolution of the Prydz Belt. J. Petrol. 48, 1443–1470.

Ludwig, K.R., 1999. Isoplot/Ex (v. 2.06)—a geochronological toolkit for Microsoft Excel. Berkeley Geochronology Center, Special Publication, No. 1a, 49 pp.

Manton, W.I., Grew, E.S., Ghofmann, J., Sheraton, J.W., 1992. Granitic rocks of the Jetty Peninsula, Amery Ice Shelf area, East Antarctica. In: Yoshida, Y., Kaminuma, K., Shiraishi, K. (Eds.), Recent Progress in Antarctic Earth Science. Terra Scientific Publishing Company, Tokyo, pp. 179–189.

Middlemost, E.A.K., 1994. Naming materials in the magma/igneous rock system. Earth Sci. Rev. 37, 215–224.

Mikhalsky, E.V., Laiba, A.A., Beliatsky, B.V., Stüwe, K., 1999. Geology, age and origin of the Mount Willing area (Prince Charles Mountains, East Antarctica). Antarct. Sci. 11, 338–352.

Mikhalsky, E.V., Sheraton, J.W., Beliatsky, B.V., 2001a. Preliminary U–Pb dating of Grove Mountains rocks: implications for the Proterozoic to Early Palaeozoic tectonic evolution of the Lambert Glacier-Prydz Bay area (East Antarctica). Terra Antarct. 8, 3–10.

Mikhalsky, E.V., Sheraton, J.W., Laiba, A.A., Tingey, R.J., Thost, D.E., Kamenev, E.N., Fedorov, L.V., 2001b. Geology of the Prince

Charles Mountains, Antarctica. AGSO Geosci. Aust. Bull. 247, 1–209.

Mikhalsky, E.V., Beliatsky, B.V., Sheraton, J.W., Roland, N.W., 2006. Two distinct Precambrian terranes in the Southern Prince Charles Mountains, East Antarctica: SHRIMP dating and geochemical constraints. Gondwana Res. 9, 291–309.

Möller, A., O'Brien, P.J., Kennedy, A., Kröner, A., 2003. The use and abuse of Th–U ratios in the interpretation of zircon. Geophys. Res. Abst. 5, 12113.

Paquette, J.L., Nédélec, A., Moine, B., Rakotondrazafy, M., 1994. U–Pb, single zircon Pb-evaporation, and Sm–Nd isotopic study of a granulite domain in SE Madagascar. J. Petrol. 102, 523–538.

Pearce, J.A., Cann, J.R., 1973. Tectonic setting of basic volcanic rocks determined using trace element analysis. Earth Planet. Sci. Lett. 19, 290–300.

Pearce, J.A., Harris, N.B.W., Tindle, A.G., 1984. Trace element discrimination diagrams for the interpretation of granitic rocks. J. Petrol. 25, 956–983.

Rubatto, D., Gebauer, D., 2000. Use of cathodoluminescence for U–Pb zircon dating by ion microprobe; some examples from the Western Alps. In: Pagel, M., Barbin, V., Blanc, P., Ohnenstetter, D. (Eds.), Cathodoluminescence in Geosciences. Springer, Berlin, pp. 373–400.

Sheraton, J.W., Black, L.P., 1988. Chemical evolution of granitic rocks in the East Antarctic Shield, with particular reference to post-orogenic granites. Lithos 21, 37–52.

Sheraton, J.W., Tindle, A.G., Tingey, R.J., 1996. Geochemistry, origin, and tectonic setting of granitic rocks of the Prince Charles Mountains, Antarctica. AGSO J. Aust. Geol. Geophys. 16, 345–370.

Shiraishi, K., Ellis, D.J., Hiroi, Y., Fanning, C.M., Motoyoshi, Y., Nakai, Y., 1994. Cambrian orogenic belt in East Antarctica and Sri Lanka: implications for Gondwana assembly. J. Geol. 102, 47–65.

Sun, S.S., McDonough, W.E., 1989. Chemical and isotopic systematics of oceanic basalts: implications for mantle composition and processes. In: Saunders, A.D., Norry, M.J. (Eds.), Magmatism in the Ocean Basins. Geological Society, pp. 313–345 (special publication).

Taylor, S.R., McLennan, S.M., 1985. The Continental Crust: Its Composition and Evolution. Blackwell, Oxford, 312 pp.

Thost, D.E., Hensen, B.J., Motoyoshi, Y., 1994. The geology of a rapidly uplifted medium and low pressure granulite facies terrane of Pan African age: the Bolingen Islands, Prydz Bay, East Antarctica. Petrology 2, 293–316.

Tingey, R.J., 1991. The regional geology of Archaean and Proterozoic rocks in Antarctica. In: Tingey, R.J. (Ed.), The Geology of Antarctica. Oxford University Press, Oxford, pp. 1–73.

Vavra, G., Gebauer, D., Schmid, R., Compston, W., 1996. Multiple zircon growth and recrystallisation during polyphase Late Carboniferous to Triassic metamorphism in granulites of Ivrea Zone (Southern Alps): an ion microprobe (SHRIMP) study. Contrib. Mineral. Petrol. 122, 337–358.

Vavra, G., Schmid, R., Gebauer, D., 1999. Internal morphology, habit and U–Th–Pb microanalysis of amphibolite-to-granulite facies zircons: geochronology of the Ivrea Zone (Southern Alps). Contrib. Mineral. Petrol. 134, 380–404.

Wang, Y., Liu, D., Ren, L., Tang, S., 2003. Advances in SHRIMP geochronology and their constraints on understanding the tectonic evolution of Larsemann Hills, East Antarctica. In: 9th International Symposium on Antarctic Earth Sciences, Potsdam, Germany, pp. 334–335.

Wang, L., He, H., Li, B., 2003. Multi-element determination in geological samples by Inductively Coupled Plasma Mass Spectrometry after fusion-precipitation treatment. Rock Mineral Anal. 22, 86–92 (in Chinese with English abstract).

Whalen, J.B., Currie, K.L., Chappell, B.W., 1987. A-type granites: geochemical characteristics, discrimination and petrogenesis. Contrib. Mineral. Petrol. 95, 407–419.

Wiedenbeck, M., Alle, P., Corfu, F., Griffin, W.L., Meier, M., Oberli, F., von Quadt, A., Roddick, J.C., Spiegel, W., 1995. Three natural zircon standards for U–Th–Pb, Lu-Hf, trace element and REE analyses. Geostand. Newslett. 19, 1–23.

Williams, I.S., 1998. U–Th–Pb geochronology by ion microprobe. Applications of Microanalytical Techniques to Understanding Mineralizing Processes. In: McKibben, M.A., Shanks, W.C., Ridley, W.I. (Eds.), Rev. Econ. Geol. 7, 1–35.

Williams, I.S., Claesson, S., 1987. Isotopic evidence for the Precambrian provenance and Caledonian metamorphism of high grade paragneisses from the Seve Nappes, Scandinavian Caledonides: II. Ion microprobe zircon U–Th–Pb. Contrib. Mineral. Petrol. 97, 205–217.

Wilson, T.J., Grunow, A.M., Hanson, R.E., 1997. Gondwana assembly: the view from southern Africa and East Gondwana. J. Geodynam. 23, 263–286.

Winchester, J.A., Floyd, P.A., 1977. Geochemical discrimination of different magma series and their differentiation products using immobile elements. Chem. Geol. 20, 325–343.

Yoshida, M., 1995. Cambrian orogenic belt in East Antarctica and Sri Lanka: implications for Gondwana assembly: a discussion. J. Geol. 103, 467–468.

Yoshida, M., Jacobs, J., Santosh, M., Rajesh, H.M., 2003. Role of Pan-African events in the Circum-East Antarctic Orogen of East Gondwana: a critical overview. In: Yoshida, M., Windley, B., Dasgupta, S. (Eds.), Proterozoic East Gondwana: Supercontinent Assembly and Breakup, vol. 206. Geological Society, London, pp. 57–75 (special publication).

Young, D.N., Black, L.P., 1991. U–Pb zircon dating of Proterozoic igneous charnockites from the Mawson Coast, East Antarctica. Antarct. Sci. 3, 205–216.

Young, D.N., Zhao, J.-x., Ellis, D.J., McCulloch, M.T., 1997. Geochemical and Sr–Nd isotopic mapping of source provinces for the Mawson charnockites, East Antarctica: implications for Proterozoic tectonics and Gondwana reconstruction. Precambrian Res. 86, 1–19.

Yuan, H.L., Gao, S., Liu, X.M., Li, H.M., Gunther, D., Wu, F.Y., 2004. Accurate U–Pb age and trace element determinations of zircon by laser ablation-inductively coupled plasma mass spectrometry. Geostand. Newslett. 28, 353–370.

Zhang, L., Tong, L., Liu, X.H., Scharer, U., 1996. Conventional U–Pb age of the high-grade metamorphic rocks in the Larsemann Hills, East Antarctica. In: Pang, Z., Zhang, J., Sun, J. (Eds.), Advances in Solid Earth Sciences. Science Press, Beijing, pp. 27–35.

Zhao, Y., Song, B., Wang, Y., Ren, L., Li, J., Chen, T., 1992. Geochronology of the late granite in the Larsemann Hills, East Antarctica. In: Yoshida, Y., Kaminuma, K., Shiraishi, K. (Eds.), Recent Progress in Antarctic Earth Science. Terra Scientific Publishing Company, Tokyo, pp. 155–161.

Zhao, Y., Liu, X.H., Song, B., Zhang, Z., Li, J., Yao, Y., Wang, Y., 1995. Constraints on the stratigraphic age of metasedimentary rocks from the Larsemann Hills, East Antarctica: possible implications for Neoproterozoic tectonics. Precambrian Res. 75, 175–188.

Zhao, J.-X., Ellis, D.E., Kilpatrick, J.A., McCulloch, M.T., 1997. Geochemical and Sr–Nd isotopic study of charnockites and related rocks in the northern Prince Charles Mountains, East Antarctica:

implications for charnockite petrogenesis and Proterozoic crustal evolution. Precambrian Res. 81, 37–66.

Zhao, Y., Liu, X.C, Fanning, C.M., Liu, X.H., 2000. The Grove Mountains, a segment of a Pan-African orogenic belt in East Antarctica. Abstract volume of the 31st IGC, Rio De Janeiro, Brazil.

Zhao, Y., Liu, X.H., Liu, X.C., Song, B., 2003. Pan-African events in Prydz Bay, East Antarctica and its inference on East Gondwana tectonics. In: Yoshida, M., Windley, B., Dasgupta, S. (Eds.), Proterozoic East Gondwana: Supercontinent Assembly and Breakup, vol. 206. Geological Society, London, pp. 231–245 (special publication).